Am J Cancer Res 2022;12(9):4160-4176
www.ajcr.us /ISSN:2156-6976/ajcr0143355

Original Article

Prediction of tumor recurrence by distinct immunoprofiles in liver transplant patients based on mass cytometry

Xuyong Wei[1,3*], Wentao Xie[1,2,3*], Weiwei Yin[4*], Mengfan Yang[1,2,3*], Abdul Rehman Khan[1,2,3], Renyi Su[1,3], Wenzhi Shu[1,3], Binhua Pan[1,2,3], Guanghan Fan[1,2,3], Kun Wang[1,2,3], Fan Yang[1,3], Di Lu[1,3], Changbiao Li[1,3], Linhui Pan[1,3], Beini Cen[1,3], Haiyang Xie[2,3], Li Zhuang[5], Shusen Zheng[2,3,5], Xun Zeng[6,10], Wei Chen[4,7,8,10], Xiao Xu[1,3,9]

[1]Department of Hepatobiliary and Pancreatic Surgery, Center for Integrated Oncology and Precision Medicine, Affiliated Hangzhou First People's Hospital, Zhejiang University School of Medicine, Hangzhou 310006, China; [2]Department of Hepatobiliary and Pancreatic Surgery, The First Affiliated Hospital, Zhejiang University School of Medicine, Hangzhou 310003, China; [3]NHFPC Key Laboratory of Combined Multi-Organ Transplantation, Hangzhou 310003, China; [4]Key Laboratory for Biomedical Engineering of The Ministry of Education, College of Biomedical Engineering and Instrument Science, Zhejiang University, Hangzhou 310058, China; [5]Department of Hepatobiliary and Pancreatic Surgery, Shulan (Hangzhou) Hospital, Hangzhou 310004, China; [6]State Key Laboratory for Diagnosis and Treatment of Infectious Diseases, National Clinical Research Center for Infectious Diseases, The First Affiliated Hospital, Zhejiang University School of Medicine, Hangzhou 310003, China; [7]Department of Cell Biology and Department of Cardiology of the Second Affiliated Hospital, Zhejiang University School of Medicine, Hangzhou 310058, China; [8]State Key Laboratory for Modern Optical Instrumentation, Department of Cell Biology, Zhejiang University, Hangzhou 310058, China; [9]Zhejiang University Cancer Center, Hangzhou 310003, China; [10]Collaborative Innovation Center for Diagnosis and Treatment of Infectious Diseases, Hangzhou 310003, China. [*]Equal contributors.

Received April 6, 2022; Accepted August 7, 2022; Epub September 15, 2022; Published September 30, 2022

Abstract: Recurrence of hepatocellular carcinoma (HCC) after liver transplantation (LT) is a marker of poor prognosis. However, the reliable biomarkers of post-LT HCC recurrence remain to be identified. In this study, serial peripheral blood samples from the LT recipients with and without HCC recurrence were collected at five time points. Single-cell mass cytomertry (CyTOF) was utilized for the in-depth analysis of peripheral blood monocellular cells (PBMCs). CyTOF analysis showed that at 3 weeks post-LT, the activated immune cell population was increased, while the fraction of immune cells with suppressive functions (myeloid-derived suppressive cells) was reduced. The post-LT immune composition in patients with LT for HCC was enormously different from that in patients with LT for causes other than HCC. Furthermore, at 3 weeks after LT, compared with patients without recurrence, the patients with HCC recurrences were high in two subsets of T cells: $CD57^+$ $HLA\text{-}DR^+$ $CD8^+$ and $CD28^+\gamma\delta$. The $CD57^+$ $HLA\text{-}DR^+$ $CD8^+$ T cells presented high levels of perforin, granzyme B, and Ki-67 and displayed a highly cytotoxic and proliferative phenotype, while the $CD28^+\gamma\delta$ T cells had reduced levels of IFN-γ and, hence, were less activated compared to $CD28^-$ cells. Based on these findings, we concluded that analyzing the PBMCs of LT recipients by CyTOF can predict the post-LT HCC recurrence. The distinct immune features can stratify patients with the risk of HCC recurrence at 3 weeks after LT, which will help clinician in further management plan and improve the prognosis of patients.

Keywords: Hepatocellular carcinoma, liver transplantation, mass cytometry

Introduction

Primary liver cancer is the sixth most common cancer and the third leading cause of cancer-related deaths worldwide. Hepatocellular carcinoma (HCC), the most common type of primary liver cancer, accounts for 75-85% of these cases. A liver transplant (LT) is the most effective treatment option in selected candidates as it removes the tumor together with the diseased organ [1, 2]. Despite the strict selection criteria, a significant fraction of patients (around 20%) experience tumor recurrence [3, 4]. Recurrence has a severe negative impact on the OS, with

the median survival time of 8.7 months [5]. Therefore, it is crucial to accurately predict the risk of recurrence so that an effective management approach can be applied to improve the OS of HCC patients with LT. Currently, the pathological parameters, such as tumor burden (number, diameter), tumor differentiation, vascular invasion, alpha-fetoprotein level, are widely used for the risk predictors of recurrence [6-10]. As these parameters exclusively focus on the pre-transplant state of the HCC patients, the effect from LT surgery and post-LT management is not considered, which leads to the low predicting power [8]. An effective approach that combines the impact of LT and post-LT management, the tumor stage, and the clinical state of the patients will be more reliable to predict the recurrence.

Immune system actively shapes not only the post-transplant outcomes (acceptance and rejection of the allograft), but also the development of recurrence. However, the influence of immune system is complex. When a strong immune system functions in surveillance against tumor recurrence, it increases the chance of allograft rejection [11]. Therefore, monitoring the changes in the immune system can be an efficient approach for the prognostic evaluation of post-LT patients. A few immunological biomarkers have been developed to evaluate the risk of recurrence. For example, the high level of preoperative C-reactive protein (CRP) and the higher neutrophil-to-lymphocyte ratio (NLR) (specifically, NLR ≥5) are associated with the worse prognosis and the increased risk of recurrence among HCC patients who underwent resection or LT [12-14].

$CD4^+$ T cell and T regulatory cell (Treg) also affect HCC recurrence after resection or LT [15-17]; however, they have not been widely adopted clinically due to low accuracy. When CRP level and Treg fraction fail to predict the post-LT HCC recurrence, higher NLR is also not accurate enough with very low specificity [13, 18, 19]. Therefore, it is an urgent need to identify explicit biomarker to predict HCC recurrence in LT patients.

The newly developed platform, Cytometry by Time-Of-Flightor (CyTOF), also known as Mass cytometry, has made the high dimensional analysis of the immune system at a single cell level possible. It also enables the real-time measurement of >40 markers on a single cell [20], a systematic profiling of the human peripheral immune atlas.

In this study, we utilized CyTOF to perform the in-depth analyses of the peripheral blood monocellular cells (PBMCs) of the LT recipients. Characterization of the dynamic immune composition of the peripheral immune system in these patients before and after LT revealed the immune features that were specific to post-LT recipients with HCC recurrence. Our study provides new insights into the post-LT immune response and assists in the construction of immune signature for the early prediction of recurrence.

Patients and methods

Clinical samples

Perioperative peripheral blood samples were collected from patients who underwent LT at SHULAN Hospital, Hangzhou, China between January 2018 and May 2019. The inclusion criteria of LT patients were: 1) over the age of 18; 2) didn't receive transcatheter arterial chemoembolization (TACE) before surgery; 3) no concurrent autoimmune disease; 4) used a standard immunosuppressive regimen in SHULAN hospital; 5) received liver transplantation for the first time; 6) received modified piggyback liver transplantation. The written informed consent was obtained from all patients before enrollment. Blood samples were collected from participants at 5 timepoints: before LT, 3 days, 1, 2, and 3 weeks after LT. All participants received followed-up examination. The diagnosis of tumor recurrence was based on computerized tomography (CT) scan and serum alpha-fetoprotein (AFP) level (Figure S3B). The study protocol was approved by the ethics committee of SHULAN hospital.

Immunosuppression regimen

For HCC-LT recipients, basiliximab was administered on the day of surgery and the fourth day after surgery for induction therapy. Tacrolimus and mycophenolate mofetil were used regularly, while methylprednisolone was only used when needed. During surgery, a high-dose steroid (MP1000 mg) was administrated (Figure S3A). Tacrolimus was administered within 4 days after LT at a concentration of 8-12 ng/ml

and was used at 7-10 ng/ml in the first month after LT. Mycophenolate mofetil was administered 2 days after LT at a dosage of 1.5 g/d. Non-HCC-LT recipients received the same tacrolimus and mycophenolate mofetil administration, but additional methylprednisolone was given from the first day after LT at a starting dose of 120 mg/12 h, which was gradually reduced to 16 mg/d in a week.

Blood sample processing

Blood samples were collected in EDTA tubes (BD) and stored at 4°C. Ficoll density gradient centrifugation (GE Healthcare) was used to separate PBMCs from EDTA-treated whole blood, and the PBMCs were kept in frozen medium (10% DMSO plus 90% FBS) until further use.

Single-cell suspension preparation

The frozen PBMCs were thawed in RPMI 1640 medium (BasalMedia) containing 1 mM glutamine (Gibco), 2 mM nonessential amino acids (Gibco), 5% heat-inactivated fetal calf serum, 10 mM HEPES (Invitrogen), penicillin/streptomycin (Gibco), and 25 units/mL benzonase nuclease (Sigma-Aldrich), and the PBMCs pellet was obtained by centrifugation. Cold Cell Staining Buffer (CSB, PBS with 0.5% bovine serum albumin) was used to wash and resuspend the pellet before staining.

Antibodies and antibody labeling

The information of the antibody used in this study was summarized in Tables S1 and S2. The MaxPAR antibody Labelling kit (Fluidigm) was used to label antibodies with metal tags. The concentration of metal labeled antibodies was assessed by Nano-100 (Thermo Scientific). An antibody stabilizer buffer was used to adjust the concentration of the labeled antibodies to 0.2 mg/ml.

Cell staining

The single cell suspension was stained for viability with 194Pt (Fluidigm) in PBS for 5 min on ice, washed, and incubated with Fc blocking mix for 20 min to reduce the non-specific staining. The samples were then stained with cell-surface antibodies for 30 min on ice, washed, and incubated in DNA Intercalator-Ir (Fluidigm) overnight to discriminate single nucleated cells from doublets. Next, the samples were stained with intracellular antibodies for 30 min on ice. Each sample was barcoded with a unique combination of isotopes for 30 min before pooling. Samples were stored at 4°C until analysis.

Cell collection by CyTOF

Barcoded samples were pooled and then resuspended with 20% EQ Four Element Calibration Beads (Fluidigm) to a final concentration of 1 million cells/ml in deionized water. Before data acquisition, the CyTOF instrument (Helios, Fluidigm) was calibrated by running tuning and QC procedures. The pooled samples were analyzed on the CyTOF instrument at an event rate of below 300 events/second.

CyTOF data analysis

CyTOF raw data (FCS files) were collected and normalized with the automated bead normalization method [21]. Samples were de-barcoded using a double-filtering scheme [22] with mass-tag barcoding and manually gated in FlowJo (version10.0) to retain single, living, and intact immune cells (**Figure 1**). To obtain accurate immune subset information, we applied X-shift algorithm [23] to sub-sampled cells from all samples. Specifically, a total of 20,000 cell events was randomly selected from each sample and pooled together for X-shift analysis using Java script (1.8.1). 2D heatmaps were plotted based on the normalized mean expression of all or selected markers for identified clusters (**Figure 1B**). For data visualization, t-Distributed Stochastic Neighbor Embedding (tSNE) algorithm [24] (MATLAB R2018a) was implemented with all markers. A total of 5000 cell events from each sample were randomly selected and pooled together for the final visualization (**Figure 1C**).

Statistics and bioinformatics analysis

PCA analysis was carried out in R (version 3.6.1) to visualize the overall alteration in immune profile between different groups of samples. Both paired and unpaired Students' T-test (R script, version 3.6.1) were performed to assess the frequency changes in different immune subsets. Correlation between immune subsets was examined by Pearson correlation coefficient calculated using R script (version 3.6.1).

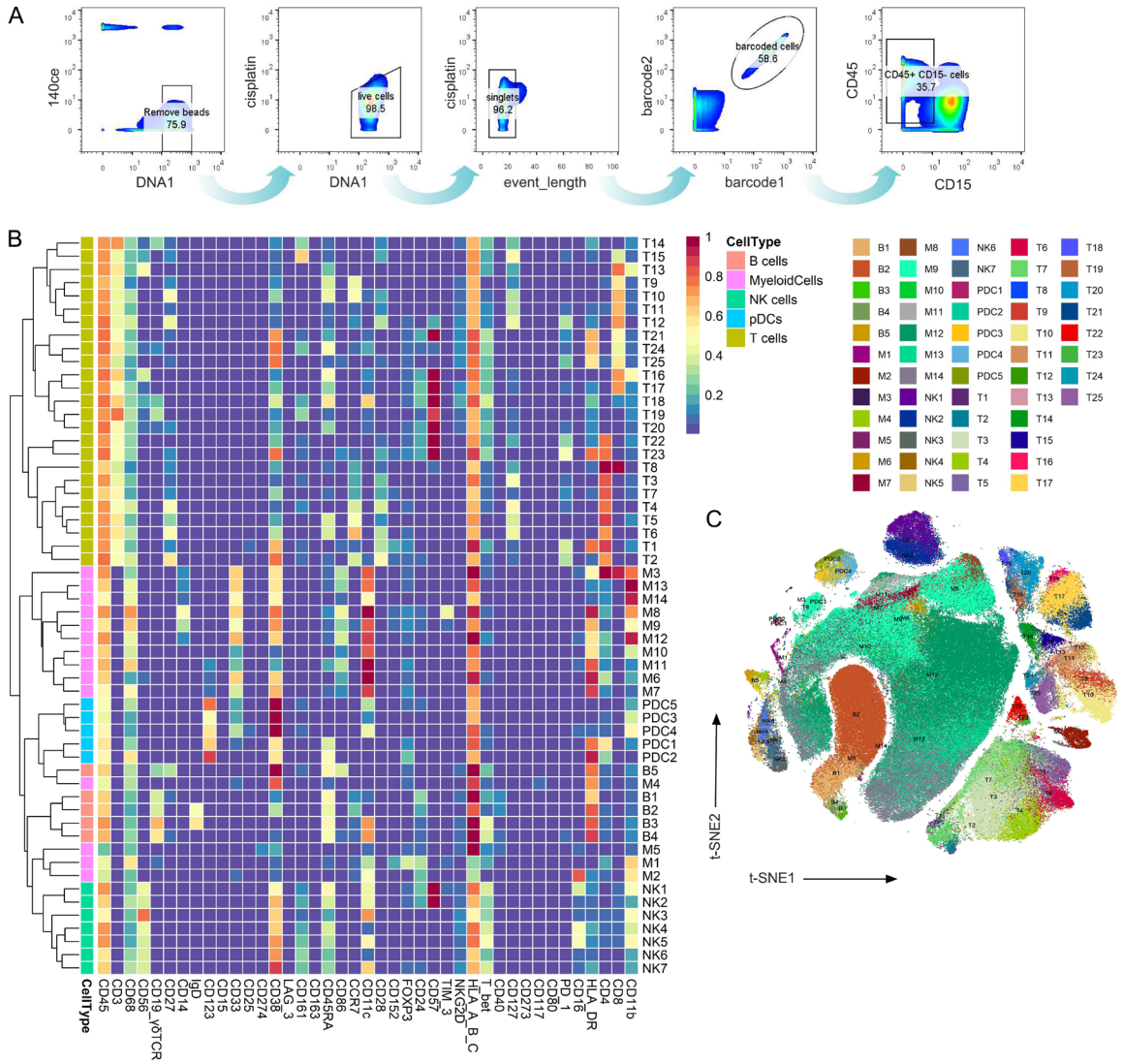

Figure 1. Immune profiles of peripheral blood monocellular cells (PBMCs) from liver transplantation recipients. A. Pseudocolor contour plot showing the gating strategy used to obtaining $CD45^+$ $CD15^-$ immune populations. B. Heatmap showing normalized mean expression of the markers of 56 X-shift-defined clusters. Clusters are grouped by expression profiles and cell types are indicated by the color (pDC: plasmacytoid dendritic cells). C. All $CD45^+$ $CD15^-$ cells are plotted on a t-SNE map colored by 56 X-shift-defined clusters.

Results

Immunophenotyping of liver transplant recipients

CyTOF was utilized to reveal the dynamic changes in the peripheral immune system of the LT recipients. A total of 49 blood samples was collected from 12 LT recipients at 5 timepoints: before surgery (BS), 3 days post-LT (D-3), 1 week post-LT (W-1), 2 weeks post-LT (W-2), and 3 weeks post-LT (W-3). All samples were subjected to CyTOF for immune profiling at a single cell level (**Figure 2A**). The demographic characteristics of these LT recipients were listed in Tables S3 and S4. Of these 12 LT recipients, 9 received LT for HCC, whereas the rest were for non-HCC.

To identify the immune signatures associated with tumor recurrence in LT recipient and to precisely profile the dynamic immune composition, the PBMCs containing more than 3 million $CD45^+$ cells were extracted from the collected samples, and a CyTOF analysis was performed using a custom-designed antibody panel with

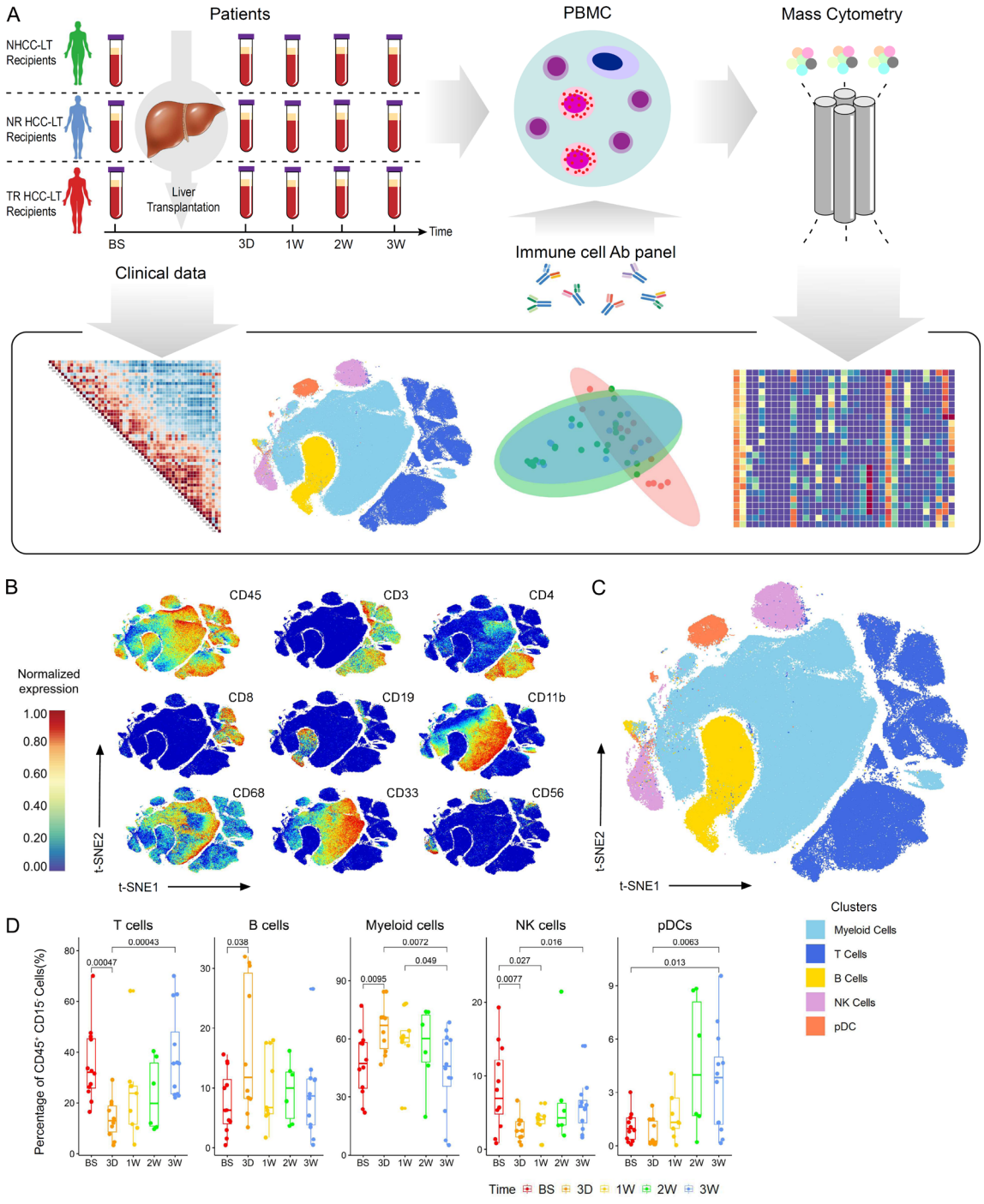

Figure 2. Immunophenotyping of peripheral blood monocellular cells (PBMCs) from liver transplantation recipients. A. Sample collection and analysis pipeline, PBMCs were collected before surgery (BS) and at 3 days (3D), 1 week (1W), 2 weeks (2W), 3 weeks (3W) after surgery from patients who received liver transplantation for hepatocellular carcinoma (HCC-LT, n=9), or other non-HCC reasons (NHCC-LT, n=3). HCC-LT recipients are classified into tumor recurrence (TR, n=4) group and non-recurrence (NR, n=5) group. Time of flight masscytometry (CyTOF) was used to analyze collected PBMCs. CyTOF results and clinical data were co-analyzed using multiple bioinformatics methods to search for immune features unique to TR HCC-LT recipients. B. Visualization of all $CD45^+$ $CD15^-$ CyTOF events from 12 enrolled liver transplantation recipients, colored by normalized expression of indicated markers. C. t-SNE map colored by main cell populations based on manual annotation of X-shift clustering. D. Box plots showing the percentage of main immune cell populations at 5 peri-transplant time points (BS, n=12; 3D, n=10; 1W, n=9; 2W, n=6; and 3W, n=12). *P*-values were calculated using unpaired two-sided Student's T-test and indicated by numbers.

42 markers (Tables S1 and S6). X-shift, an unsupervised clustering algorithm [21], was applied to manually gated $CD45^+$ $CD15^-$ immune cells (**Figure 1A**, Method), which generated 56 distinct immune subsets (**Figure 1B** and **1C**).

Based on the lineage marker expression profiles in tSNE plots [22], we identified 15 T cell subsets, 5 B cell subsets, 7 NK cell subsets, 5 plasmacytoid dendritic cell (pDCs) subsets, and 14 myeloid cell subsets (**Figures 1B**, **1C**, **2B**, **2C** and **3A**). By comparing the population of these subsets, we observed a substantial increase in myeloid cells and B cells, while a substantial decrease in T cells and NK cells in the peripheral immune system 3 days post-LT (**Figures 2D** and **3B**). These alterations were transient as the population of these cells (T cells, B cells, and myeloid cells) were gradually back to their preoperative levels by 3 weeks post-LT. However, the proportion of pDCs increased after LT and reached the peak 2 weeks post-LT (**Figure 2D**). These findings were also confirmed by plotting a series of tSNE maps on PBMCs that were extracted at different timepoints post-LT (**Figure 3C**). All these CyTOF analyses indicated the transient changes in the major immune subsets of the peripheral blood, which were returned to pre-LT levels 3 weeks after LT.

Liver transplant induced changes in peritransplant immune compositions

To depict the dynamic changes in the peripheral immune system induced by LT, we examined the alteration in the population of each immune subset by the X-shift algorithm. The PBMCs samples from 9 patients were collected at four timepoints: before surgery, 3 days post-LT (D-3), 1 week post-LT (W-1), and 3 weeks post-LT (W-3) for the paired analysis. Two subsets of plasmacytoid dendritic cells, pDC4 and pDC5 representing 37% and 23% of total pDCs, respectively (**Figure 3D**), showed a continuously significant increase at 3 weeks post-LT (**Figures 4A** and S1A). These two clusters expressed high levels of CD11c, CD123, and CD38 (**Figure 4B**). In contrast, the other three subsets of pDCs initially showed a transient decrease and then later increased during post-LT (**Figures 4A** and S1A). pDCs play a critical role in the development of immune tolerance after transplantation [25]. We previously found that pDC4 and pDC5 that were HLA-DR-CD86- and were linked with low levels of antigen presentation, were responsible for the effector T cell exhaustion and Treg induction [25]. Furthermore, we also identified four other subtypes for myeloid cells: M9, M12, M13, and M14, accounted for 15%, 45%, 13%, and 18% of total myeloid cells, respectively (**Figure 3D**). Myeloid-derived suppressor cells (MDSCs) M13 and M14 expressed low levels of CD14 and HLA-DR, though the expression levels of CD33, CD11b, CD11c, and HLA-ABC were high (**Figure 4B**). The population of M13 and M14 cells was significantly decreased at 3 weeks post-LT (**Figures 4A** and S1B), suggesting that immune activation occurred after this period. This might also be the reason of allograft rejection since MDSCs immune suppression ability dropped at this time [26, 27].

T cells, another important component of adaptive immunity, showed great heterogeneity in response to allograft. We identified 25 diverse T cell clusters, including 9 $CD4^+$, 11 $CD8^+$, and 3 γδ T cell subsets (**Figures 4C** and S2A). Among these, the composition of $CD8^+$ T cells was more affected by the LT than in other subsets. The percentage of naïve $CD8^+$ T cells (TN) decreased (*P*-Value =0.049), while the number of effective memory $CD8^+$ T cells (TEM) increased (*P*-Value =0.052) at 3 weeks post-LT, suggesting that the cell-mediated immune system was activated after LT (**Figure 4D**, top panel). Whereas these variations were not seen in the $CD4^+$ T cells (**Figure 4D**, bottom panel).

Furthermore, we observed two patterns of variation while comparing the changes in the composition of $CD8^+$ T cell clusters. One dynamic pattern was associated with T10, T11, and T15 clusters. The fraction of these $CD8^+$ T cell clusters was initially decreased at D-3 post-LT, but then recuperated at W-3 post-LT to preoperative levels (**Figures 4E** and S2A). These clusters (T10, T11, and T15) exhibited high levels of HLA-ABC, CD40, and CD127 and low levels of CD57 and HLA-DR (**Figure 4C**). The other dynamic pattern was associated with T21 and T25 clusters. Different from the previous pattern, these $CD8^+$ T cell clusters were initially expanded and reached the peak at W-3 post-LT, which was also different from the dynamics of total $CD8^+$ T cells (Figure S2B). These clusters (T21 and T25) exhibited high levels of

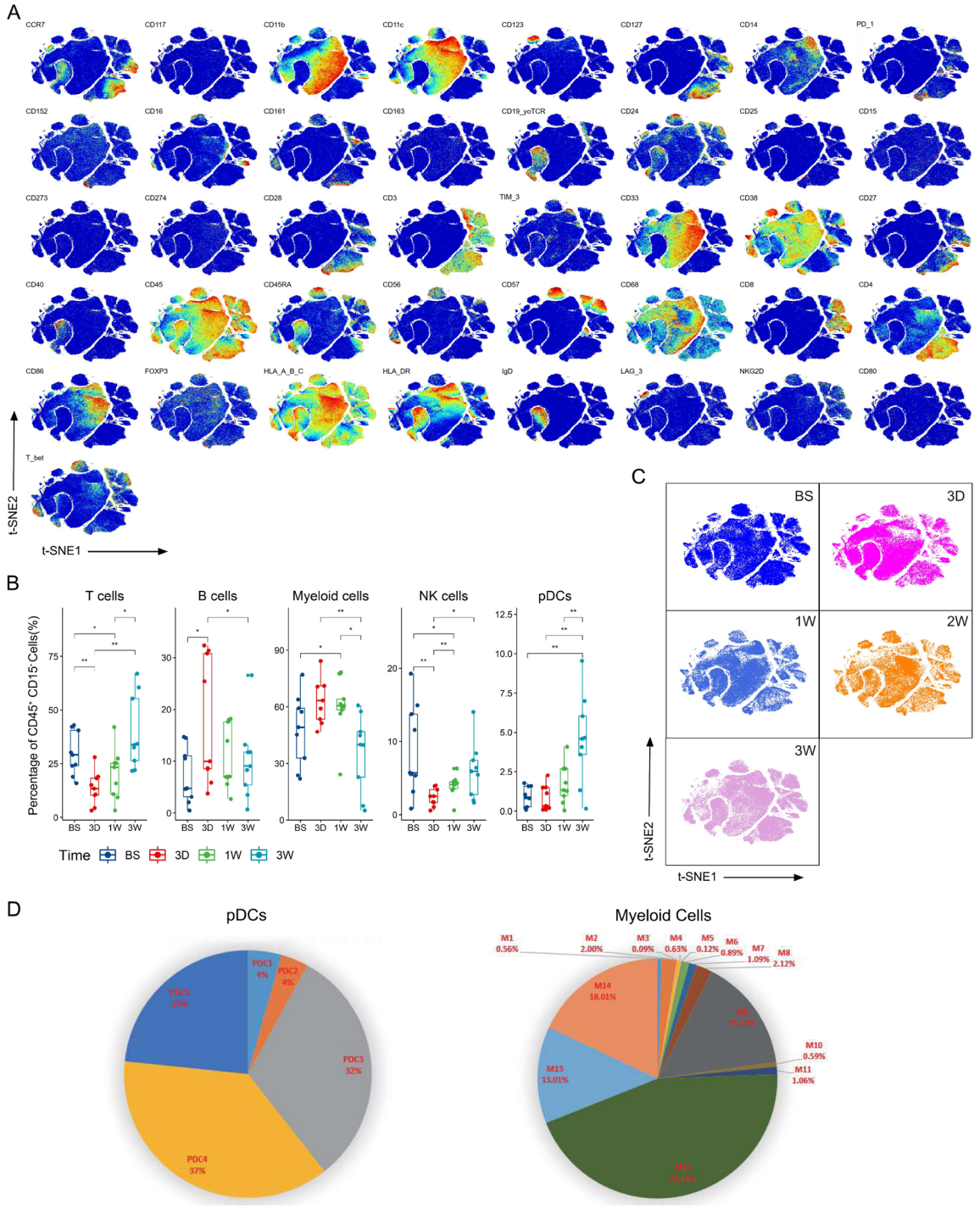

Figure 3. Immune profiles of peripheral blood monocellular cells (PBMCs) from liver transplantation recipients. A. Cells colored by normalized expression of indicated markers on the t-SNE map. B. Box plots showing the percentage of main immune cell populations at 4 peri-transplant time points (BS, 3D, 1W, and 3W), 9 patients with their PBMCs collected at all 4 time points were included. *P*-values were calculated by two-sided paired Student's T-test (*: P<0.05, **: P<0.01 and ***: P<0.001). The horizontal line of the box plot indicates the median, the boxes represent the interquartile range (IQR), and the whiskers reach the farthest data within 1.5×IQR from the median. C. Plotting PBMCs collected at 5 different time points (BS, 3D, 1W, 2W, and 3W) from liver transplantation recipients on a tSNE map reveals the peripheral immune composition changes after liver transplantation. D. Pie plot showing the composition of plasmacytoid dendritic cells (pDCs) and myeloid cells.

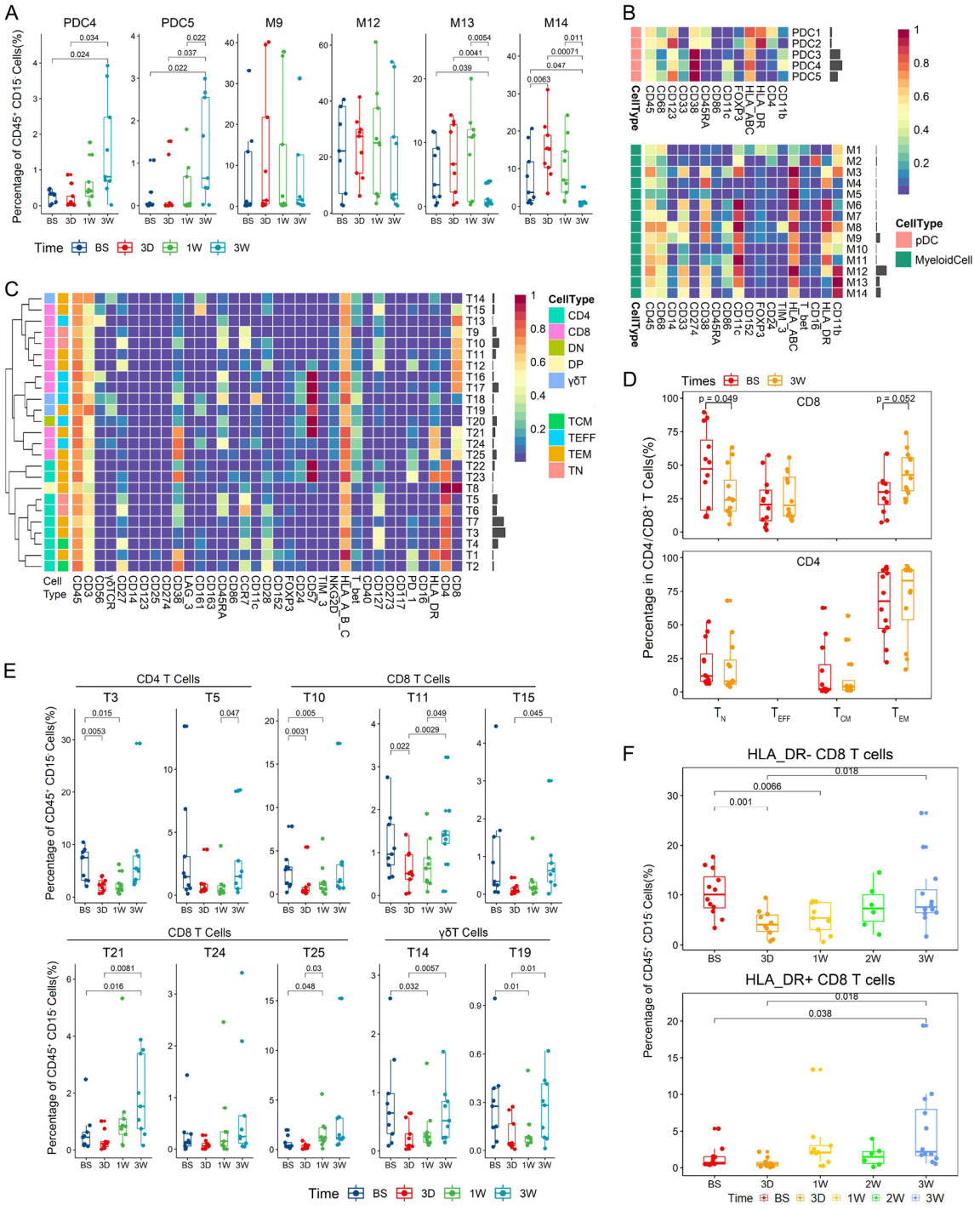

Figure 4. Peripheral immune composition change induced by liver transplantation. A. Box plots showing the percentage of indicated B cell and Myeloid cell clusters at 4 peri-transplant time points (BS, 3D, 1W, and 3W), 9 patientswith their PBMCs collected at all 4 time pointswere included. *P*-values were calculated by two-sided paired Student's T-test andindicated by numbers. B. Heatmap showing normalized marker expression of X-shift-defined B cell and Myeloid cell clusters. C. Heatmap showing normalized marker expression of X-shift-defined T cell clusters. Clusters were grouped by expression profiles and cell types were indicated by the color. D. Boxplots showing the frequencychanges of naïve T cells (TN), effector T cells (TEFF), central memory T cells (TCM), and effector memory T cells (TEM) inCD4 and CD8 T cells. *P*-values were calculated by two-sided paired Student's T-testand indicated by numbers. E. Box plots showing the percentage of indicated T cell clusters at 4 peri-transplant time points (BS, 3D, 1W, and 3W), 9 patients with their PBMCs collected at all 4 time points were included. *P*-values were calculated by two-sided paired Student's T-test andindicated by numbers. F. Box plots showing the frequency comparisons of HLA-DR$^+$/HLA-DR$^-$ CD8$^+$ T cellsat 5 peri-transplant time points (BS, 3D, 1W, 2W, and 3W). *P*-values were calculated using two-sided unpaired Student's T-testandindicated by numbers.

CD38, HLA-ABC, and HLA-DR, but had different levels of PD-1, CD57, and CD161 (**Figure 4C**). In addition, the dynamic pattern of HLA-DR$^+$ CD8$^+$ T cells was different from HLA-DR$^-$ CD8$^+$ T cells (**Figure 4F**). HLA-DR$^-$ CD8$^+$ T cells exhibited a similar pattern as the T10, T11, and T15 clusters, while the HLA-DR$^+$ CD8$^+$ T cells showed the similar changing pattern as the T21 and T25 clusters post-LT. Previous studies have reported that the expression level of CD8$^+$HLA-DR$^+$ T cells is associated with chronic immune activation [28-30]. In this study, we found the existence of the sustained activation of peripheral immune cells, which might be the main cause of allograft rejection.

CD57$^+$ HLA-DR$^+$ CD8$^+$ T cells and CD28$^+$γδ T cells were specific to tumor recurrent HCC-LT recipients

To differentiate further the tumor specific immune types and identify possible biomarker of tumor recurrence, we divided the LT recipients into three clinical sets: non-HCC LT (NHCC-LT) recipients (3 patients, 12 samples), HCC-LT recipients with tumor recurrence (TR) (4 patients, 17 samples), and HCC-LT recipients without recurrence (NR) (5 patients, 20 samples). The clinical features of all HCC-LT recipients were described in Table S5.

To explore the distribution of immune subsets among these three clinical groups, tSNE was applied. We found that NHCC-LT and HCC-LT recipients had very different immune cell composition, while there was small but evident difference between TR HCC-LT and NR HCC-LT patients (**Figure 5A**). TR HCC-LT and NR HCC-LT recipients shared a larger overlapped area (95%) of confidential ellipse when compared to NHCC-LT recipients by principal component analysis (PCA), which was in consistent with the above results (**Figure 5B**). Furthermore, PCA also showed that HCC-LT recipients had larger confidential ellipse (95%) compared to NHCC-LT, which signified the heterogeneity in the immune composition of HCC-LT recipients (**Figure 5B**).

Furthermore, comparison of the fractions of the immune cells revealed that a total of 26 immune subsets were markedly different between HCC-LT and NHCC-LT groups (**Figure 5C** top panel). Of these, 15 clusters were different before LT; however, after LT, the number of different immune clusters was significantly reduced to six at 1 and 3 weeks post-LT.

Although there were no noticeable variations between TR and NR HCC-LT groups before LT and during D-3 to W-1 post-LT (**Figure 5C**, bottom panel), two immune subsets were different at W-3 post-LT between these groups (**Figure 5C**, bottom panel). Those immune cells were T14, a γδ T cell subset, and T21, a CD8$^+$ T cells. T14 cells express high levels of CD28, CD127, CD161 and T-bet, while intermediate levels of HLA-DR and CD38, and low level of CD45RA. We observed that the T14 cells were significantly expanded in HCC-LT recipient 3 weeks post-LT, particularly in TR HCC-LT group (**Figures 5C**, **5D**, S4A, and S4B). Whereas T21 cells, a subset of CD8$^+$ T cells expressing high levels of CD57, HLA-DR, and CD38, were expanded in TR HCC-LT group compared to NRHCC-LT and NHCC-LT group at 3 weeks post-LT (**Figures 5C**, **5D**, and S4B). We also confirmed these findings via manual gating of T14 and T21 and identifying CD28$^+$ CD127$^+$ cells from γδ T cells, and CD57$^+$ HLA-DR$^+$ cells from CD8$^+$ T cells (**Figure 5E**).

Moreover, to depict the phenotype of the T21 cluster, we compared the expression levels of T cell functional markers among manually gated CD57$^+$ HLA-DR$^+$ CD8$^+$ T cells (T21) and three other manually gated CD8$^+$ T cell subsets with different expression levels of CD57 and HLA-DR. The T21 subset (CD57$^+$ HLA-DR$^+$CD8$^+$ T cells) demonstrated low expression levels of costimulatory markers CD27 and CD28, but relatively high expression levels of PD-1 and CD38 (**Figure 5F**). These data suggested that the T cells in T21 subset had the phenotype of late-stage effectors (with CD45RA+ and CCR7-) that had experienced T cell activation [31].

In-depth functional assessment of CD57$^+$ HLA-DR$^+$ CD8$^+$ T cells and CD28$^+$γδ T cells

Having identified the properties of different immune subset cells, we sought to further explore their immune mechanisms. T21 (CD57$^+$ HLA-DR$^+$ CD8$^+$ T cells), T14 (CD28$^+$γδ T cells), and peripheral blood samples were collected from 3 other HCC-LT recipients at 3 weeks post-LT, and the in-depth CyTOF functional assessment was performed (**Figure 6A**). This analysis comprised 30 cytokines and functional biomarkers (Tables S2 and S7). Data was pro-

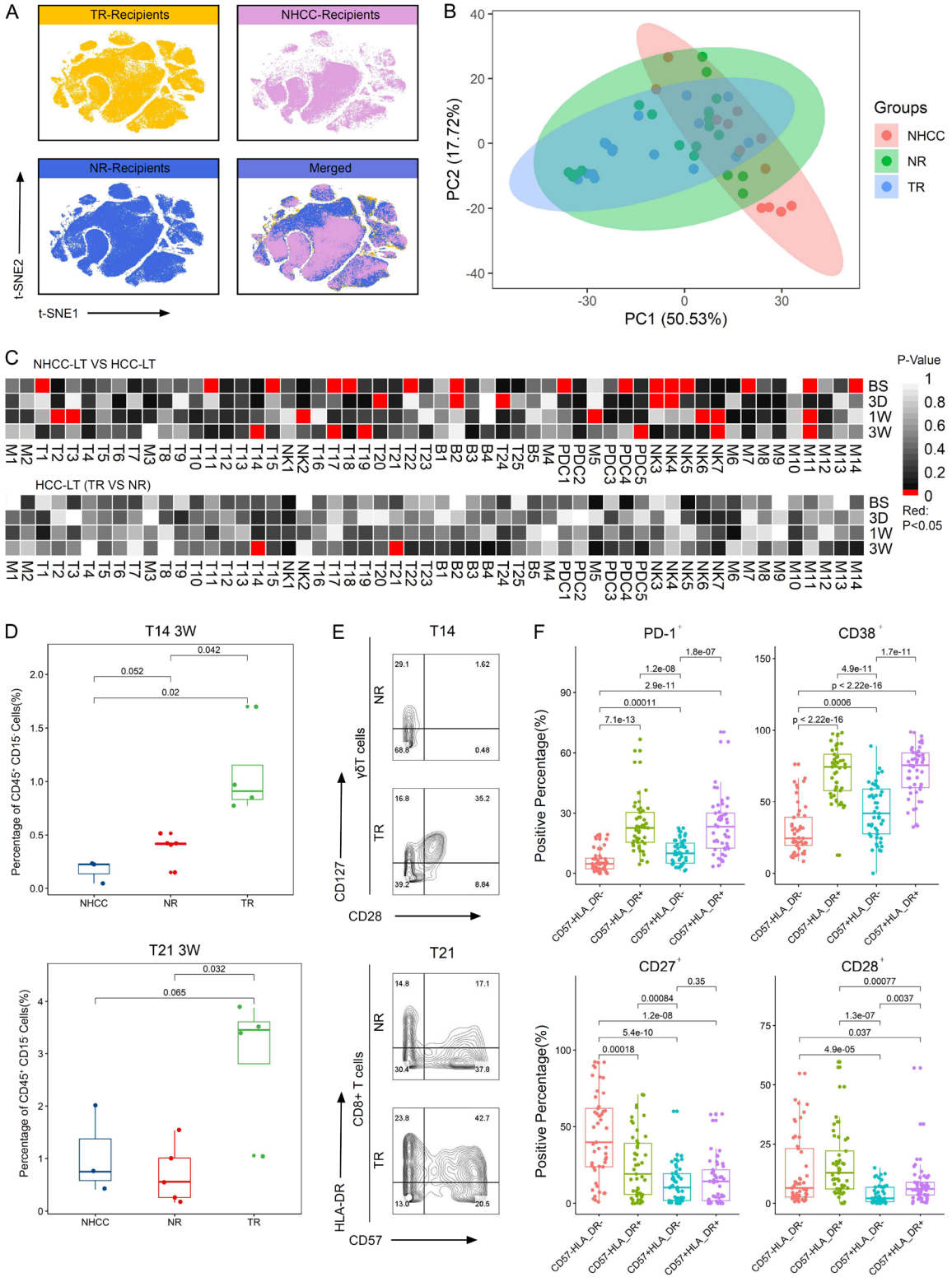

Figure 5. Identification of clusters unique to tumor recurrence LT recipients. A. tSNE map of PBMCs isolated from tumor recurrenceHCC-LT recipients (TR, orange), non-recurrenceHCC-LT recipients (NR, blue), and patients received LT not for HCC (NHCC-LT, pink). B. Principal Component Analysis of all blood samples grouped by TR (blue), NR (green), and NHCC-LT (red) recipients. The shadedarea representedthe 95% confidential ellipseof each sample group. C. Heatmap depicting the immune composition difference between (1) NHCC-LT and HCC-LT recipients (up) and between (2) TR HCC-LT and NR HCC-LT (bottom) recipients. Heatmaps were colored by *P*-values calculated using

two-sided unpaired Student's T-test. Each unit of the heatmap represents the significance of the immune composition difference for the indicated cluster at the indicated time point and was painted to red if *P*-value <0.05. D. Box plots showing the frequency comparisonsof cluster T14 (up) and T21 (bottom) in NHCC recipients, TR recipients, and NR recipients at 3 weeks after transplantation. *P*-values are calculated using two-sided unpaired Student's T-test andindicated by numbers. E. Biaxial plots showing manually gated T14 and T21 from representative samples. T14 was manually gated by high expression of CD28 and CD127 (up), T21 was manually gated by high expression of CD57 and HLA-DR (bottom). F. Box plots showing the positive percentages of PD-1/CD38/CD27/CD28 in 4 groups divided according to the expression of CD57 and HLA-DR. *P*-values were calculated using two-sided paired Student's T-test andindicated by numbers.

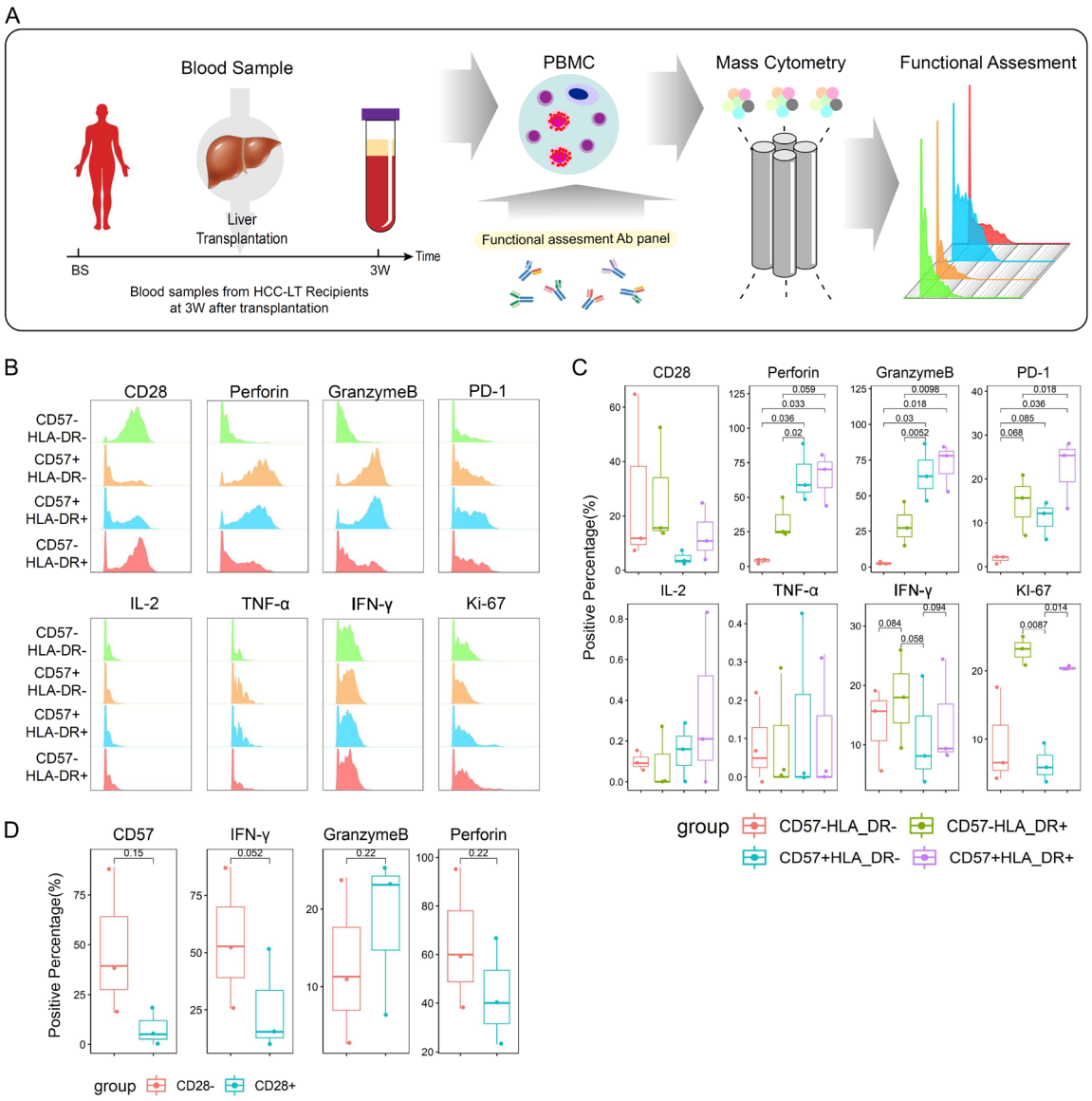

Figure 6. Functional assessment of CD57⁺ HLA-DR⁺ CD8⁺ T cells and CD28⁺γδ T cells using CyTOF. A. Sample collection and analysis pipeline, PBMCs were collected 3 weeks (3W) after transplantation from patients who received liver transplantation for hepatocellular carcinoma (HCC-LT, n=3). Collected PBMCs were analyzed by Time of flight mass-cytometry (CyTOF) using a specially designed 30-maker functional assessment panel. B. Histograms showing the expressiondistributions of indicated cytokines and functional biomarkers in 4 divided groups: CD57⁻ HLA-DR⁻ CD8⁺ T cells, CD57⁻ HLA-DR⁺ CD8⁺ T cells, CD57⁺ HLA-DR⁻ CD8⁺ T cells, and CD57⁺ HLA-DR⁺ CD8⁺ T cells. C. Boxplots showing the positive percentages of the indicated cytokines and functional biomarkersin 4 CD8⁺ T cell subsets divided according to the expression of CD57 and HLA-DR. *P*-values were calculated using two-sided paired Student's T-testandindicated by numbers. D. Boxplots showing the positive percentages of the indicated cytokines and functional biomarkersin 2 γδ T cell subsets divided according to the expression of CD28. *P*-values were calculated using two-sided paired Student's T-test andindicated by numbers.

cessed, and $CD8^+$ T cells were segregated into 4 parts based on the expression levels of CD57 and HLA-DR (Figure S5A), while γδ T cells were segregated into 2 parts based on the expression levels of CD28 T cells, on manual gating (Figure S6). We found that $CD57^+$ $CD8^+$ T cells (T21 cluster) displayed low level of costimulatory receptor (CD28) but considerably high levels of cytotoxic makers (perforin and granzyme B) as compared to $CD57^-$ $CD8^+$ T cells (**Figure 6B** and **6C**). Furthermore, $CD57^+$ HLA-DR^+ $CD8^+$ T cells (T21) expressed higher level of Ki-67 than $CD57^+$ HLA-DR^- $CD8^+$ T cells, suggesting the high proliferation rate of $CD57^+$ HLA-DR^+ $CD8^+$ T cells. This subset also expressed the highest level of PD-1 among all four $CD8^+$ T cells groups (**Figure 6C**). Collectively, these findings suggested $CD57^+$ HLA-DR^+ $CD8^+$ T cells were highly proliferative and cytotoxic T cells. In contrast, $CD28^+$γδ T cells expressed lower level of IFN-γ than $CD28^-$γδ T cells, suggesting a less cytotoxic phenotype (**Figure 6D**).

Systematic correlation analysis revealed immune subsets relationships specific to HCC-LT recipients with tumor recurrence

To determine the key immune regulators involved in tumor recurrence and reveal the immunological differences between TR HCC-LT and NR HCC-LT recipients, a complete association analysis of all identified immune clusters was performed. A triangle correlation heat-map was constructed, which revealed several differences between TRHCC-LT and NR HCC-LT recipients (**Figure 7A**). For example, many noticeable association patterns in the NR HCC-LT group (as indicated in the red box in **Figure 7A**) were not detectable in the TRHCC-LT group, while many insignificant associations in the NRHCC-LT group (as indicated in the green box in **Figure 7A**) were enhanced in the TR HCC-LT group.

Furthermore, the correlations of T14 and T21 immune subsets with other clusters were studied in the TR HCC-LT recipients. As shown in **Figure 7A** and **7B**, T22 ($CD57^+$ HLA-DR^- PD-1+ $CD4^+$ T cells) and T23 ($CD57^+$ HLA-DR^+ PD-1+ $CD4^+$ T cells) were closely correlated with T21 ($CD57^+$ HLA-DR^+ $CD8^+$ T cells) in TR HCC-LT recipients. Similarly, there was a substantial association between T14 ($CD28^+$γδ T cells) and T12 ($CD27^+$ $CD28^+$ HLA-DR^+ $CD4^+$ T cells) in TR HCC-LT recipients. In contrast, all these associations were not detected in the NR HCC-LT recipients. Similarly, a substantial association between pDC4 ($CD11b^+$ $CD11c^+$ CD38hipDCs) and T14 in NRHCC-LT recipients was observed which was not present in TR HCC-LT recipients (**Figure 7B**).

Taken together, all these findings validated the robust interactions among immune subsets, explicitly those that were reinforced in the TRHCC-LT recipients, suggesting their potential role as a biomarker in the prediction of recurrences among HCC-LT recipients.

Discussion

Liver resection and LT are the most effective curative treatment options for localized HCC. However, the prognosis of HCC remains poor due to the high recurrence rate of HCC. Early prediction of recurrence will be critical to improve the prognosis of HCC.

Immune environment after LT has long been linked with the prognosis of recipients. Here, we used CyTOF at single-cell level and performed comprehensive phenotyping of PBMCs among LT recipients.

Single-cell mass cytometry was performed to identify differences between tolerant pediatric liver transplant recipients and recipients who are stable on single-agent immunosuppression. High-dimensional phenotypic analysis revealed distinct immunoprofiles between transplant populations as well as a $CD4^+$ T cell subset of operational tolerance ($CD4^+$ $CD5^+$ $CD25^+$ $CD38^-$/lo CD45RA) that correlated with tolerance in pediatric recipients [32]. Study also demonstrated an imaging mass cytometry panel of 10 validated markers was developed to explore the feasibility in characterizing the immune landscape of chronic rejection obtained from adult liver transplant recipients [33]. Thus, mass cytometry has been determined to have the potential to detect new biomarkers, identify therapeutic targets, and generate patient-specific predictive models of clinical outcomes in solid organ transplantation [34, 35].

Our analysis elucidated the transient as well as sustained changes in the peripheral immune system composition in patients 3 weeks post-LT. Two immune subsets that might assist in

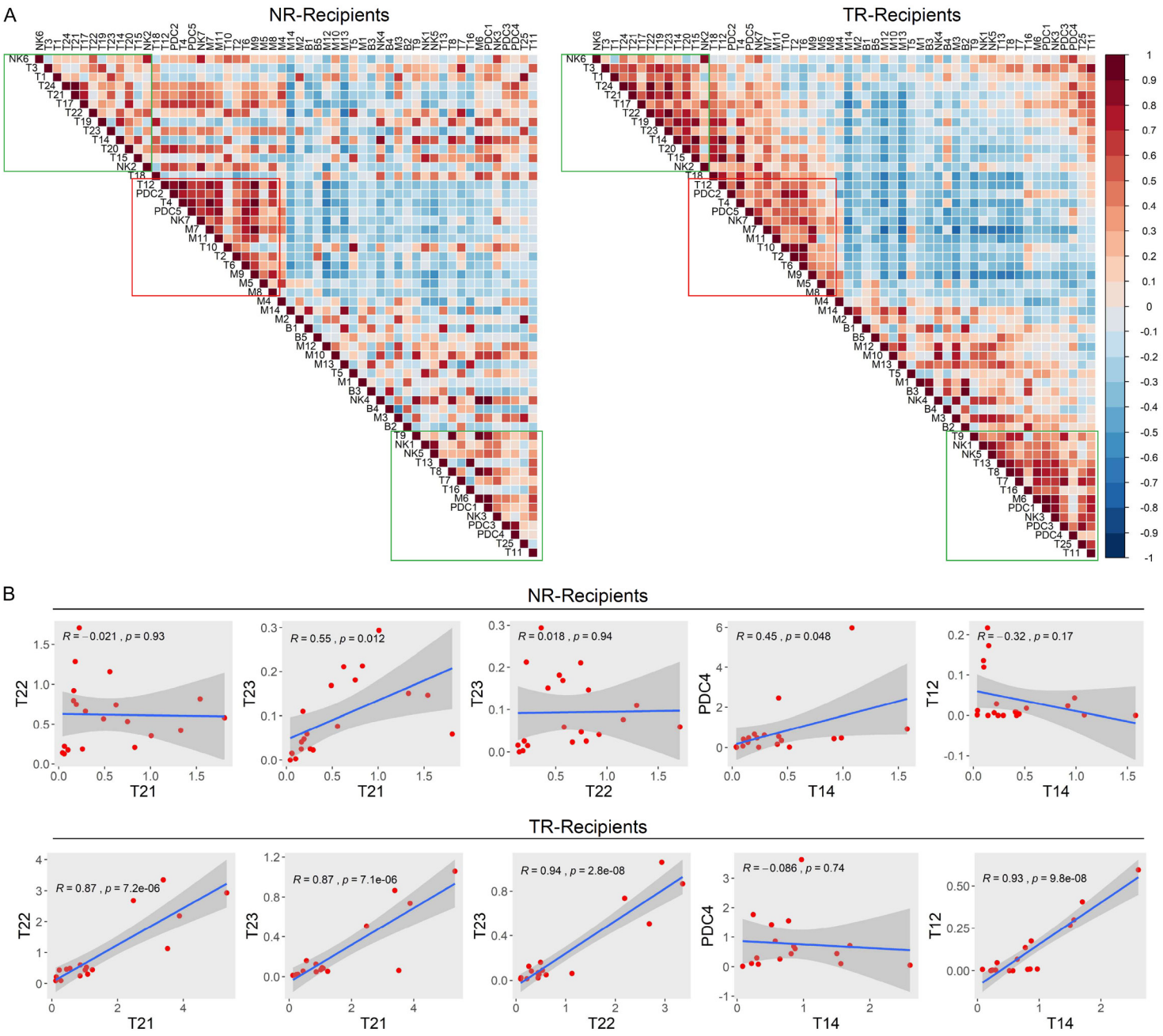
A
NR-Recipients
TR-Recipients
B
NR-Recipients
R = −0.021 , p = 0.93
R = 0.55 , p = 0.012
R = 0.018 , p = 0.94
R = 0.45 , p = 0.048
R = −0.32 , p = 0.17
TR-Recipients
R = 0.87 , p = 7.2e-06
R = 0.87 , p = 7.1e-06
R = 0.94 , p = 2.8e-08
R = −0.086 , p = 0.74
R = 0.93 , p = 9.8e-08

Figure 7. Correlation Analysis of X-shift-defined immune clusters in tumor recurrence (TR) and non-recurrence (NR) recipients. A. Heatmap showing pairwise Pearson correlation coefficients of immune cell phenotypes in TR and NR groups. Green rectangles indicatedstrong correlations unique to TR recipients. The red rectangle indicatedstrong correlations unique to NR recipients. B. Scatterplots showing strong correlations unique to TR or NR groups. Pearson correlations and *P* Values were indicated.

the early prediction of HCC among post-LT recipient were also identified, and their immune features were demonstrated.

As previous studies have focused on the limited number of immune subsets [36], we carried out an in-depth profiling of the peripheral immune system in LT recipients. We discovered a series of dynamic changes in several immune subsets. The fraction of activated T cells (i.e., $CD8^+$ TEM, HLA-DR^+ $CD8^+$ T cells) was increased, while the number of suppressive immune cells (MDSCs) was decreased post-LT (**Figures 4A**, **4D**, and S1).

Importantly, we identified two immune subsets ($CD57^+$ HLA-DR^+ $CD8^+$ T cells and $CD28^+$γδ T cells) that differed considerably between LT recipient with and without recurrence at 3 weeks post-LT (**Figure 5C-E**), although there was no difference in the total immune signatures (**Figure 5A-C**). These two immune subsets were found at higher level in the post-LT patients with the recurrence than without recurrence. We speculated these two subsets were the tumor-sensitive immune subsets induced by anti-tumor response in a low tumor burden environment. Indeed, single-cell mass CyTOF analysis of the peripheral immune system revealed that distinct responses in the LT recipient with HCC recurrence could be detected as early as 3 weeks after LT.

In addition, we discovered a tumor-specific $CD28^+$γδ T cell subset with high expression levels of CD27, CD127, CD161, T-bet, and HLA-DR, and low expression level of CD45RA (**Figure 4C**). Previously, CD45RA-$CD27^+$γδ T cells were defined as central memory (TCM) subsets [37]. CD21 is essential for the growth of IFN-γ-producing γδ T cells in infection models [38]. $CD27^+$γδ T cells secrete IFN-γ and are different from $CD27^-$γδ T cells [39]. CD28 is crucial for the survival, proliferation, and cytokine production of γδ T cells [40, 41]. Growing evidence has proven that γδ T cells have anti-tumor as well as pro-tumor activities. Although γδ T cells can constrain tumor growth by secreting inflammatory cytokines including IFN-γ and TNF-α [42], γδ T cells can promote tumor growth via the production of IL-17 and the recruitment of MDSCs in the tumor microenvironment [43].

$CD28^+$γδ T cells had high CD27 and T-bet levels, suggesting the involvement of γδ T cell subset in preventing tumor recurrence in LT recipients. Our results also suggested that T14 subset, a central memory γδ T cell (TCM) subset, had anti-tumor action in response to the low tumor burden environment in peripheral blood of TR HCC-LT recipients. Nevertheless, further study is needed to determine the exact type of antigen that $CD28^+$γδ T cells recognizes, and whether $CD28^+$γδ T cells can be utilized as possible immunotherapy target against tumor recurrence.

Furthermore, the number of activated $CD8^+$ T cells expressing high levels of activation markers, such as CD57, CD38 and HLA-DR, was explicitly high in TR HCC-LT recipients at 3 weeks post-LT (**Figure 4C**). These T cells also expressed high levels of cytotoxic markers, such as Granzyme B and perforin, exhibiting a hyperactive and cytotoxic phenotype. These findings are in consistent with previous reports of high $CD8^+$ CD57+ T cells in patients with AIDS and pulmonary tuberculosis [44, 45].

$CD8^+$ $CD57^+$ T cells are known to undergo oligoclonal expansion and exert immunosuppressive activity in organ transplant patients [46]. Their clonal increase has also been reported in autoimmune diseases, infectious diseases, cancer, and allograft transplantation [47]. $CD8^+$ $CD57^+$ T cells have also been reported to have impaired proliferation [48]. Conversely, we found that expression levels of Ki-67 and PD-1 were higher in HLA-DR^+ $CD57^+$ $CD8^+$ T cells than in HLA-DR^- counterparts (**Figure 6C**), suggesting that their active role was possibly due to their interaction with the tumor or allograft antigens. This proliferation of cytotoxic HLA-DR^+ $CD57^+$ $CD8^+$ T cells in TR recipients indicated the primary immune response against tumor. We also found that unlike $CD28^+$γδ T cells, the population of HLA-DR^+ $CD57^+$ $CD8^+$ T cells was only expanded in the LT recipient with HCC

recurrence, while their population in the NHCC-LT patients and LT recipient without tumor recurrence was similar before and after surgery. These data suggested that tumor antigen was essential for the expansion of this subset (**Figure 5D**), which was only present in TR HCC-LT recipients but not in NR HCC-LT nor in LT patients without recurrence. Although the role of HLA-DR$^+$ CD57$^+$ CD8$^+$ T cells in the evolution of tumor recurrence is still not clear and needs further study, our findings suggested that these two immune subsets might serve as diagnostic biomarkers of tumor recurrence in HCC-LT recipients as early as 3 weeks post-LT.

There are several limitations in this study. First, the number of HCC patient (n=12) enrolled in this study was small, and only a few (n=4) developed tumor recurrence after LT. Hence, our findings should be further validated on a large cohort of HCC-LT recipients. Second, samples collected from more timepoints will provide more detailed information on the immune landscape of HCC-LT patients. Nevertheless, by performing immunophenotyping using single-cell CyTOF, we revealed the comprehensive changes in the immune arena of patients with LT. Single-cell CyTOF could be an effective approach to identify immune diagnostic signature for the early prediction of post-LT tumor recurrence.

Acknowledgements

This work was supported by the Chinese National Science & Technology Major Project (No. 2017ZX10203205); National Natural Science Funds for Distinguished Young Scholar of China (No. 81625003); Key Program, National Natural Science Foundation of China (No. 81930016); and the Key Research & Development Plan of Zhejiang Province (No. 2019C03050).

Disclosure of conflict of interest

None.

Address correspondence to: Dr. Xiao Xu, Department of Hepatobiliary and Pancreatic Surgery, Affiliated Hangzhou First People's Hospital, Zhejiang University School of Medicine, Huansha Road, Hangzhou 310006, China. E-mail: zjxu@zju.edu.cn; Dr. Wei Chen, Department of Cell Biology, School of Medicine, Zhejiang University, Hangzhou, China. E-mail: jackweichen@zju.edu.cn; Dr. Xun Zeng, School of Medicine, Zhejiang University, Hangzhou, China. E-mail: xunzeng@zju.edu.cn

References

[1] Zaydfudim VM, Vachharajani N, Klintmalm GB, Jarnagin WR, Hemming AW, Doyle MB, Cavaness KM, Chapman WC and Nagorney DM. Liver resection and transplantation for patients with hepatocellular carcinoma beyond milan criteria. Ann Surg 2016; 264: 650-658.

[2] Bruix J and Sherman M; American Association for the Study of Liver Diseases. Management of hepatocellular carcinoma: an update. Hepatology 2011; 53: 1020-1022.

[3] Sapisochin G and Bruix J. Liver transplantation for hepatocellular carcinoma: outcomes and novel surgical approaches. Nat Rev Gastroenterol Hepatol 2017; 14: 203-217.

[4] Yang Z, Wang S, Tian XY, Xie QF, Zhuang L, Li QY, Chen CZ and Zheng SS. Impact of treatment modalities on patients with recurrent hepatocellular carcinoma after liver transplantation: preliminary experience. Hepatobiliary Pancreat Dis Int 2020; 19: 365-370.

[5] Tabrizian P, Jibara G, Shrager B, Schwartz M and Roayaie S. Recurrence of hepatocellular cancer after resection: patterns, treatments, and prognosis. Ann Surg 2015; 261: 947-955.

[6] Halazun KJ, Najjar M, Abdelmessih RM, Samstein B, Griesemer AD, Guarrera JV, Kato T, Verna EC, Emond JC and Brown RS Jr. Recurrence after liver transplantation for hepatocellular carcinoma: a new MORAL to the story. Ann Surg 2017; 265: 557-564.

[7] Decaens T, Roudot-Thoraval F, Badran H, Wolf P, Durand F, Adam R, Boillot O, Vanlemmens C, Gugenheim J, Dharancy S, Bernard PH, Boudjema K, Calmus Y, Hardwigsen J, Ducerf C, Pageaux GP, Hilleret MN, Chazouilleres O, Cherqui D, Mallat A and Duvoux C. Impact of tumour differentiation to select patients before liver transplantation for hepatocellular carcinoma. Liver Int 2011; 31: 792-801.

[8] Verna EC, Patel YA, Aggarwal A, Desai AP, Frenette C, Pillai AA, Salgia R, Seetharam A, Sharma P, Sherman C, Tsoulfas G and Yao FY. Liver transplantation for hepatocellular carcinoma: Management after the transplant. Am J Transplant 2020; 20: 333-347.

[9] Mehta N, Heimbach J, Harnois DM, Sapisochin G, Dodge JL, Lee D, Burns JM, Sanchez W, Greig PD, Grant DR, Roberts JP and Yao FY. Validation of a Risk Estimation of Tumor Recurrence After Transplant (RETREAT) score for hepatocellular carcinoma recurrence after liver transplant. JAMA Oncol 2017; 3: 493-500.

[10] Gao F, Zhu HK, Zhu YB, Shan QN, Ling Q, Wei XY, Xie HY, Zhou L, Xu X and Zheng SS. Predictive value of tumor markers in patients with recurrent hepatocellular carcinoma in different vascular invasion pattern. Hepatobiliary Pancreat Dis Int 2016; 15: 371-377.
[11] Zarrinpar A and Busuttil RW. Liver transplantation: past, present and future. Nat Rev Gastroenterol Hepatol 2013; 10: 434-440.
[12] Hashimoto K, Ikeda Y, Korenaga D, Tanoue K, Hamatake M, Kawasaki K, Yamaoka T, Iwatani Y, Akazawa K and Takenaka K. The impact of preoperative serum C-reactive protein on the prognosis of patients with hepatocellular carcinoma. Cancer 2005; 103: 1856-1864.
[13] Gomez D, Farid S, Malik HZ, Young AL, Toogood GJ, Lodge JP and Prasad KR. Preoperative neutrophil-to-lymphocyte ratio as a prognostic predictor after curative resection for hepatocellular carcinoma. World J Surg 2008; 32: 1757-1762.
[14] Xu ZG YC, Liu LX, Wu G, Zhao ZX, Wang YZ, Shi BQ, Wang YH. The pretransplant neutrophil-lymphocyte ratio as a new prognostic predictor after liver transplantation for hepatocellular cancer: a systematic review and meta-analysis. Biomark Med 2018 Feb; 12: 189-199.
[15] Li CX, Ling CC, Shao Y, Xu A, Li XC, Ng KT, Liu XB, Ma YY, Qi X, Liu H, Liu J, Yeung OW, Yang XX, Liu QS, Lam YF, Zhai Y, Lo CM and Man K. CXCL10/CXCR3 signaling mobilized-regulatory T cells promote liver tumor recurrence after transplantation. J Hepatol 2016; 65: 944-952.
[16] Confer BD, Choudhary M, Lopez R and Zein NN. Monitoring serial CD4(+) T-cell function after liver transplantation can be used to predict hepatocellular carcinoma recurrence. Transplant Proc 2015; 47: 217-222.
[17] Zhang W, Zhong H, Zhuang L, Yu J, Xu X, Wang W, Zhang M, Zhou L and Zheng S. Peripheral blood CD4(+) cell ATP activity measurement to predict HCC recurrence post-DCD liver transplant. Int J Clin Pract 2016; 70 Suppl 185: 11-16.
[18] Unitt E, Marshall A, Gelson W, Rushbrook SM, Davies S, Vowler SL, Morris LS, Coleman N and Alexander GJ. Tumour lymphocytic infiltrate and recurrence of hepatocellular carcinoma following liver transplantation. J Hepatol 2006; 45: 246-253.
[19] Bertuzzo VR, Cescon M, Ravaioli M, Grazi GL, Ercolani G, Del Gaudio M, Cucchetti A, D'Errico-Grigioni A, Golfieri R and Pinna AD. Analysis of factors affecting recurrence of hepatocellular carcinoma after liver transplantation with a special focus on inflammation markers. Transplantation 2011; 91: 1279-1285.
[20] Spitzer Matthew H and Nolan Garry P. Mass cytometry: single cells, many features. Cell 2016; 165: 780-791.
[21] Finck R, Simonds EF, Jager A, Krishnaswamy S, Sachs K, Fantl W, Pe'er D, Nolan GP and Bendall SC. Normalization of mass cytometry data with bead standards. Cytometry A 2013; 83: 483-494.
[22] Zunder ER, Finck R, Behbehani GK, Amir el AD, Krishnaswamy S, Gonzalez VD, Lorang CG, Bjornson Z, Spitzer MH, Bodenmiller B, Fantl WJ, Pe'er D and Nolan GP. Palladium-based mass tag cell barcoding with a doublet-filtering scheme and single-cell deconvolution algorithm. Nat Protoc 2015; 10: 316-333.
[23] Samusik N, Good Z, Spitzer MH, Davis KL and Nolan GP. Automated mapping of phenotype space with single-cell data. Nat Methods 2016; 13: 493-496.
[24] Amir el AD, Davis KL, Tadmor MD, Simonds EF, Levine JH, Bendall SC, Shenfeld DK, Krishnaswamy S, Nolan GP and Pe'er D. viSNE enables visualization of high dimensional single-cell data and reveals phenotypic heterogeneity of leukemia. Nat Biotechnol 2013; 31: 545-552.
[25] Rogers NM, Isenberg JS and Thomson AW. Plasmacytoid dendritic cells: no longer an enigma and now key to transplant tolerance? Am J Transplant 2013; 13: 1125-1133.
[26] Kumar V, Patel S, Tcyganov E and Gabrilovich DI. The nature of myeloid-derived suppressor cells in the tumor microenvironment. Trends Immunol 2016; 37: 208-220.
[27] Zhang W, Li J, Qi G, Tu G, Yang C and Xu M. Myeloid-derived suppressor cells in transplantation: the dawn of cell therapy. J Transl Med 2018; 16: 19.
[28] Imamichi H, Lempicki RA, Adelsberger JW, Hasley RB, Rosenberg A, Roby G, Rehm CA, Nelson A, Krishnan S, Pavlick M, Woods CJ, Baseler MW and Lane HC. The CD8+HLA-DR+ T cells expanded in HIV-1 infection are qualitatively identical to those from healthy controls. Eur J Immunol 2012; 42: 2608-20.
[29] Speiser DE, Migliaccio M, Pittet MJ, Valmori D, Liénard D, Lejeune F, Reichenbach P, Guillaume P, Lüscher I, Cerottini JC and Romero P. Human CD8(+) T cells expressing HLA-DR and CD28 show telomerase activity and are distinct from cytolytic effector T cells. Eur J Immunol 2001; 31: 459-466.
[30] Zubkova I, Duan H, Wells F, Mostowski H, Chang E, Pirollo K, Krawczynski K, Lanford R and Major M. Hepatitis C virus clearance correlates with HLA-DR expression on proliferating CD8+ T cells in immune-primed chimpanzees. Hepatology 2014; 59: 803-813.
[31] Powell DJ Jr, Dudley ME, Robbins PF and Rosenberg SA. Transition of late-stage effector T cells to CD27+ CD28+ tumor-reactive effector memory T cells in humans after adoptive cell transfer therapy. Blood 2005; 105: 241-250.

[32] Lau AH, Vitalone MJ, Haas K, Shawler T, Esquivel CO, Berquist WE, Martinez OM, Castillo RO and Krams SM. Mass cytometry reveals a distinct immunoprofile of operational tolerance in pediatric liver transplantation. Pediatr Transplant 2016; 20: 1072-1080.

[33] Ung N, Goldbeck C, Man C, Hoeflich J, Sun R, Barbetta A, Matasci N, Katz J, Lee JSH, Chopra S, Asgharzadeh S, Warren M, Sher L, Kohli R, Akbari O, Genyk Y and Emamaullee J. Adaptation of imaging mass cytometry to explore the single cell alloimmune landscape of liver transplant rejection. Front Immunol 2022; 13: 831103.

[34] Christophersen A, Lund EG, Snir O, Sola E, Kanduri C, Dahal-Koirala S, Zuhlke S, Molberg O, Utz PJ, Rohani-Pichavant M, Simard JF, Dekker CL, Lundin KEA, Sollid LM and Davis MM. Distinct phenotype of CD4(+) T cells driving celiac disease identified in multiple autoimmune conditions. Nat Med 2019; 25: 734-737.

[35] Slepicka PF, Yazdanifar M and Bertaina A. Harnessing mechanisms of immune tolerance to improve outcomes in solid organ transplantation: a review. Front Immunol 2021; 12: 688460.

[36] Fujiki M, Esquivel CO, Martinez OM, Strober S, Uemoto S and Krams SM. Induced tolerance to rat liver allografts involves the apoptosis of intragraft T cells and the generation of CD4(+) CD25(+)FoxP3(+) T regulatory cells. Liver Transpl 2010; 16: 147-154.

[37] Dieli F, Poccia F, Lipp M, Sireci G, Caccamo N, Di Sano C and Salerno A. Differentiation of effector/memory Vdelta2 T cells and migratory routes in lymph nodes or inflammatory sites. J Exp Med 2003; 198: 391-397.

[38] Annunziato F, Cosmi L, Santarlasci V, Maggi L, Liotta F, Mazzinghi B, Parente E, Fili L, Ferri S, Frosali F, Giudici F, Romagnani P, Parronchi P, Tonelli F, Maggi E and Romagnani S. Phenotypic and functional features of human Th17 cells. J Exp Med 2007; 204: 1849-1861.

[39] Ribot JC, deBarros A, Pang DJ, Neves JF, Peperzak V, Roberts SJ, Girardi M, Borst J, Hayday AC, Pennington DJ and Silva-Santos B. CD27 is a thymic determinant of the balance between interferon-gamma- and interleukin 17-producing gammadelta T cell subsets. Nat Immunol 2009; 10: 427-436.

[40] Ribot JC, debarros A and Silva-Santos B. Searching for "signal 2": costimulation requirements of gammadelta T cells. Cell Mol Life Sci 2011; 68: 2345-2355.

[41] Ribot JC and Silva-Santos B. Differentiation and activation of gammadelta T Lymphocytes: focus on CD27 and CD28 costimulatory receptors. Adv Exp Med Biol 2013; 785: 95-105.

[42] Paul S and Lal G. Regulatory and effector functions of gamma-delta (gammadelta) T cells and their therapeutic potential in adoptive cellular therapy for cancer. Int J Cancer 2016; 139: 976-985.

[43] Coffelt SB, Kersten K, Doornebal CW, Weiden J, Vrijland K, Hau CS, Verstegen NJM, Ciampricotti M, Hawinkels LJAC, Jonkers J and de Visser KE. IL-17-producing gammadelta T cells and neutrophils conspire to promote breast cancer metastasis. Nature 2015; 522: 345-348.

[44] Sada-Ovalle I, Torre-Bouscoulet L, Valdez-Vazquez R, Martinez-Cairo S, Zenteno E and Lascurain R. Characterization of a cytotoxic CD57+ T cell subset from patients with pulmonary tuberculosis. Clin Immunol 2006; 121: 314-323.

[45] Le Priol Y, Puthier D, Lecureuil C, Combadiere C, Debre P, Nguyen C and Combadiere B. High cytotoxic and specific migratory potencies of senescent CD8+ CD57+ cells in HIV-infected and uninfected individuals. J Immunol 2006; 177: 5145-5154.

[46] Strioga M, Pasukoniene V and Characiejus D. CD8+ CD28- and CD8+ CD57+ T cells and their role in health and disease. Immunology 2011; 134: 17-32.

[47] Focosi D, Bestagno M, Burrone O and Petrini M. CD57+ T lymphocytes and functional immune deficiency. J Leukoc Biol 2010; 87: 107-116.

[48] Brenchley JM, Karandikar NJ, Betts MR, Ambrozak DR, Hill BJ, Crotty LE, Casazza JP, Kuruppu J, Migueles SA, Connors M, Roederer M, Douek DC and Koup RA. Expression of CD57 defines replicative senescence and antigen-induced apoptotic death of CD8+ T cells. Blood 2003; 101: 2711-2720.

Table S1. CyTOF panels 42 makers panel used in the experiment

Biomarkers		Biomarkers	
CD3	T cell	CD80	Costimulatar-L
CD4	$CD4^+$T cell	CD86	Costimulatar-L
CD8	$CD8^+$T cell	CD123	pDC
CD11b	Myeloid cells	CD127	IL7-R
CD11c	DC	CD161	Th17, NK
CD15	granulocytes	CD163	M2
CD14	LPS-R	CD273	PD-L2
CD16	NK, granulocytes	CD274	PD-L1
CD19	B cells	PD-1	Coinhibitory-R
CD24	Breg	CTLA-4	Coinhibitory-R
CD25	Treg	TIM-3	Coinhibitory-R
CD27	Costimulatar-R, Breg	LAG-3	Coinhibitory-R
CD28	Costimulatar-R	FOXP3	Treg
CD33	MDSC	HLA-A/B/C	HLA-I
CD38	cADP enzyme	HLA-DR	HLA-II
CD40	Costimulatar-R	γδTCR	γδ T cells
CD45	leukocyte	NKG2D	NK cell
CD45RA	Naïve cell	T-Bet	Th1
CD56	NK cells	CCR7	T_{CM}
CD57	NK cells	IgD	Naïve B cells
CD68	Macrophage	CD117	c-kit

Table S2. CyTOF panels 30 makers panel used in the functional assessment

Biomarkers		Biomarkers	
CD3	T cell	IL-1b	Cytokine
CD4	CD4 T cell	IL-2	Cytokine
CD8	CD8 T cell	IL-4	Cytokine
CD11b	Myeloid cells	IL-8	Cytokine
CD11c	DC	IL-9	Cytokine
CD20	B Cell	IL-10	Cytokine
CD28	Costimulatar-R	IL-13	Cytokine
CD33	MDSC	IL-17a	Cytokine
CD38	cADP enzyme	IL-21	Cytokine
CD45	leukocyte	PD-1	Coinhibitory-R
CD57	B3GAT1	Ki-67	Proliferation
CD68	Macrophage	TNF-α	Cytokine
CD123	pDC	Perforin	Cytotoxicity
γδTCR	γδT cell	Granzyme B	Cytotoxicity
HLA-DR	HLA-II	IFN-γ	Cytokine

Table S3. Detailed patient information P1-P9, HCC-LT recipients; P10-P12, NHCC-LT recipients

	Age	Male	Billirubin (μmol/L)	Albumin (g/L)	INR	WBC (10^9/L)	Creatinine (μmol/L)	Encephal-opathy	Ascites	MELD score	ALT	AST
P1	43	0	50	30.5	1.34	1.9	48	0	0	6.76	43	92
P2	36	1	21	45.4	1.32	4.7	67	0	0	2.19	41	57
P3	35	1	215	32.2	1.43	13.3	75	0	1	24.48	9	52
P4	61	1	30	33.1	1.26	2.5	56	0	0	3.18	44	77
P5	54	1	14	45.7	1.16	5.7	62	0	0	-3.31	45	31
P6	43	1	40	35.4	1.65	1.7	62	0	0	9.17	28	40
P7	62	1	64	43.7	1.79	15.9	111	0	0	19.65	669	1025
P8	28	1	23	39.3	1.16	8.1	73	0	0	2.63	83	111
P9	49	1	34	42.7	1.52	5.5	86	0	1	10.13	23	568
P10	42	1	145	33.7	2.74	9.1	51	1	1	23.29	239	601
P11	40	1	173	35.1	2.95	12.9	44	1	1	24.11	907	183
P12	67	0	114	30.5	4.27	16	142	1	0	35.09	174	350

Table S4. Demographics of Patient Cohort, liver function, and other laboratory examination result

Demographic factor	HCC-LT recipients (n=9)	NHCC-LT recipients (n=3)
Age	45.67±11.14	49.67±12.28
Male	8 (89%)	2 (67%)
Billirubin (μmol/L)	54.56±58.55	144.00±24.10
Albumin (g/L)	38.67±5.65	33.10±1.93
INR	1.40±0.20	3.32±0.68
WBC (10^9/L)	6.59±4.74	12.67±2.82
Creatinine (μmol/L)	71.11±17.57	79.00±44.64
Encephalopathy	0	3 (100%)
Ascites	2 (22%)	2 (67%)
MELD score	8.32±8.35	27.50±5.38
ALT (U/L)	109.44±198.76	440.00±331.28
AST (U/L)	228.11±323.21	378.00±171.79

INR: International Normalized Ratio, WBC: White Blood Cell (Count), MELD: Model for end-stage liver disease, calculated as: MELD = 3.78×ln [serum bilirubin (mg/dL)] + 11.2×ln[INR] + 9.57×ln [serum creatinine (mg/dL)] + 6.43, ALT: Alanine amino-transferase, AST: Aspartate aminotransferase.

Table S5. Oncological characteristic of patients received liver transplantation for hepatocellular carcinoma

Oncology characteristics	Tumor recurrence recipients (n=4)	Non-recurrence recipients (n=5)
Age	39.00±8.28	51.20±10.19
Male	75%	100%
MELD Score	11.00±8.22	6.18±7.81
AFP	33203.25±26884.79	74.70±120.04
Tumor number		
1	1 (25%)	2 (40%)
2	0	0
≥3	3 (75%)	3 (60%)
Maximum diameter(cm)	4.50±1.50	3.84±1.96
Differentiation		
poor	3 (75%)	1 (20%)
intermediate	1 (25%)	3 (60%)
well	0	1 (20%)
MVI		
M0	0	4 (80%)
M1	1 (25%)	0
M2	3 (75%)	1 (20%)
Within Millan Criteria	0	1 (20%)
Within Hangzhou Criteria	0	3 (60%)

MELD: Model for end-stage liver disease, AFP: Alpha fetal protein, MVI: microvascular invasion. Millan Criteria: Single nodule no larger than 5 cm, or up to 3 nodules no larger than 3 cm. Hangzhou Criteria: Tumor burden up to 8 cm, or AFP up to 400 ng/ml, and well-moderate differentiation.

Table S6. Antibody information Mass-tags, clone, brands of antibodies used in the CyTOF experiment

No.	mass-tag	antibody	Clone	Brand
1	89Y	CD45	HI30	BioLegend
2	115In	CD3	UCHT1	BioXcell
3	139La	CD68	Y1/82A	BioLegend
4	141Pr	CD56	NCAM16.2	BD biosciences
5	142Nd	γδTCR	5A6.E9	home-made
6	142Nd	CD19	HIB19	BioLegend
7	143Nd	CD27	O323	BioLegend
8	144Nd	CD14	M5E2	BioLegend
9	145Nd	IgD	IA6-2	BioLegend
10	146Nd	CD123	6H6	BioLegend
11	147Sm	CD15	W6D3	BioLegend
12	148Nd	CD33	WM53	BioLegend
13	149Sm	CD25	24212	R&D Systems
14	150Nd	CD274 (PD-L1)	29E.2A3	BioLegend
15	151Eu	CD38	HIT2	BioLegend
16	152Sm	LAG-3 (CD223)	874501	R&D Systems
17	153Eu	CD161	HP-3G10	BioLegend
18	154Sm	CD163	GHI/61	BioLegend
19	155Gd	CD45RA	HI100	BioLegend
20	156Gd	CD86	Fun-1	BD biosciences
21	158Gd	CD197 (CCR7)	G043H7	BioLegend
22	159Tb	CD11c	BU15	BioLegend
23	160Gd	CD28	CD28.2	BioLegend
24	161Dy	CD152 (CTLA-4)	14D3	eBioscience
25	162Dy	FOXP3	PCH101	eBioscience
26	163Dy	CD24	ML5	BioLegend
27	164Dy	CD57	HCD57	BioLegend
28	165Ho	TIM-3 (CD366)	F38-2E2	BioLegend
29	166Er	NKG2D (CD314)	1D11	BioLegend
30	167Er	HLA-A/B/C	W6/32	BioLegend
31	168Er	T-Bet	4B10	BioLegend
32	169Tm	CD40	82111	R&D Systems
33	170Er	CD127 (IL-7Ra)	A019D5	BioLegend
34	171Yb	CD273	24F.10C12	BioLegend
35	172Yb	CD117 (c-kit)	104D2	BioLegend
36	173Yb	CD80	2D10.4	eBioscience
37	174Yb	CD279 (PD-1)	EH12.2H7	BioLegend
38	175Lu	CD16	3G8	BioLegend
39	176Yb	HLA-DR	L243	BioLegend
40	197Au	CD4	RPA-T4	BioLegend
41	198Pt	CD8	RPA-T8	BioLegend
42	209Bi	CD11b	M1/70	home-made

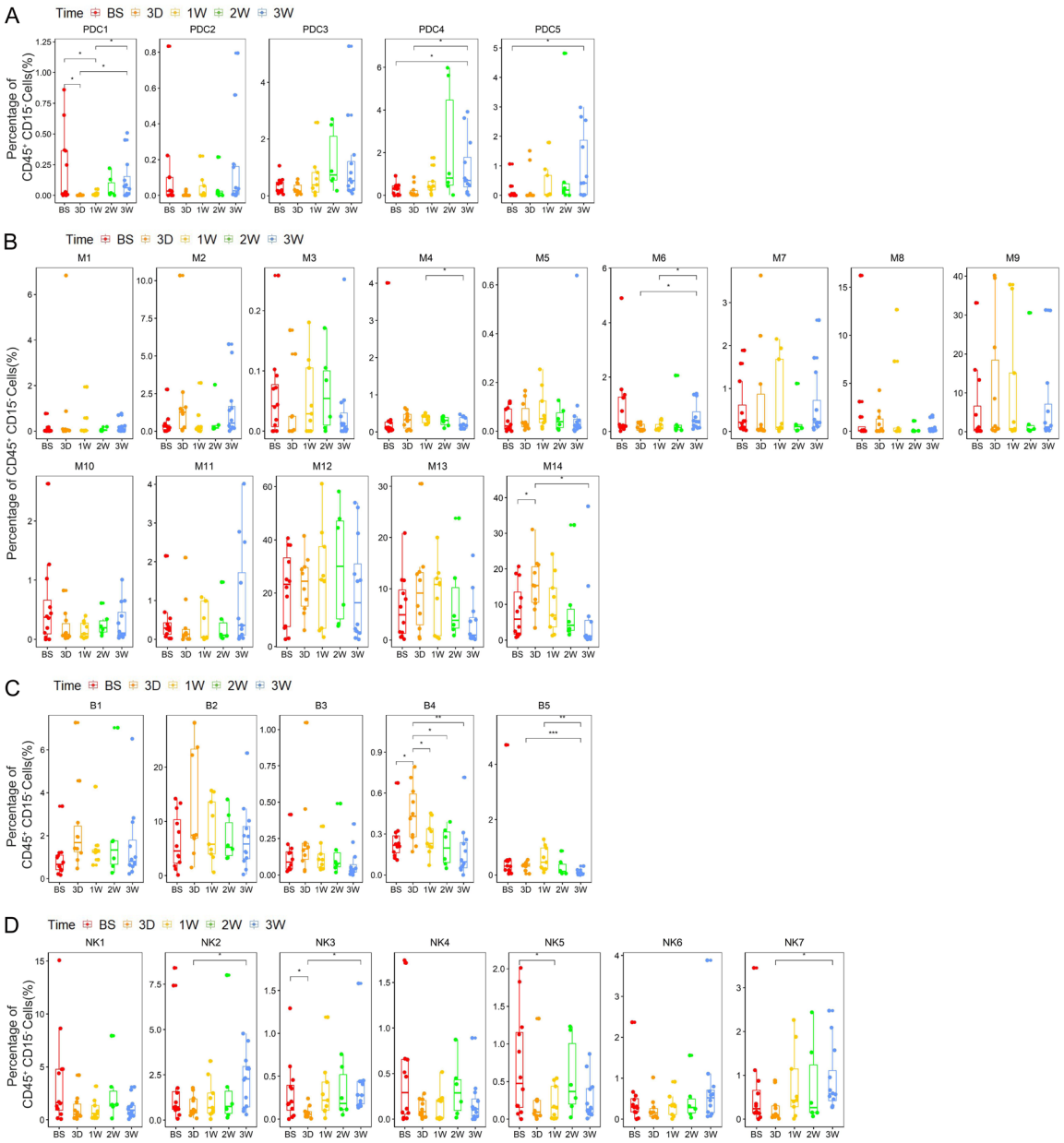

Figure S1. The frequency change of X-shift-defined immune subsets. Box plots showed the percentage of indicated immune cell subsets at 5 peri-transplant time points (BS, 3D, 1W, 2W, and 3W), *P*-values were calculated by two-sided unpaired Student's T-tes t(*: P<0.05, **: P<0.01 and ***: P<0.001) The horizontal line of the box plot indicates the median, the boxes represent the interquartile range (IQR), and the whiskers reach to the farthest data within 1.5×IQR from the median. A: The frequency change of 5 plasmacytoid dendritic cell subsets. B: The frequency change of 14 myeloid cell subsets. C: The frequency change of 5 B cell subsets. D: The frequency change of 7 NK cell subsets.

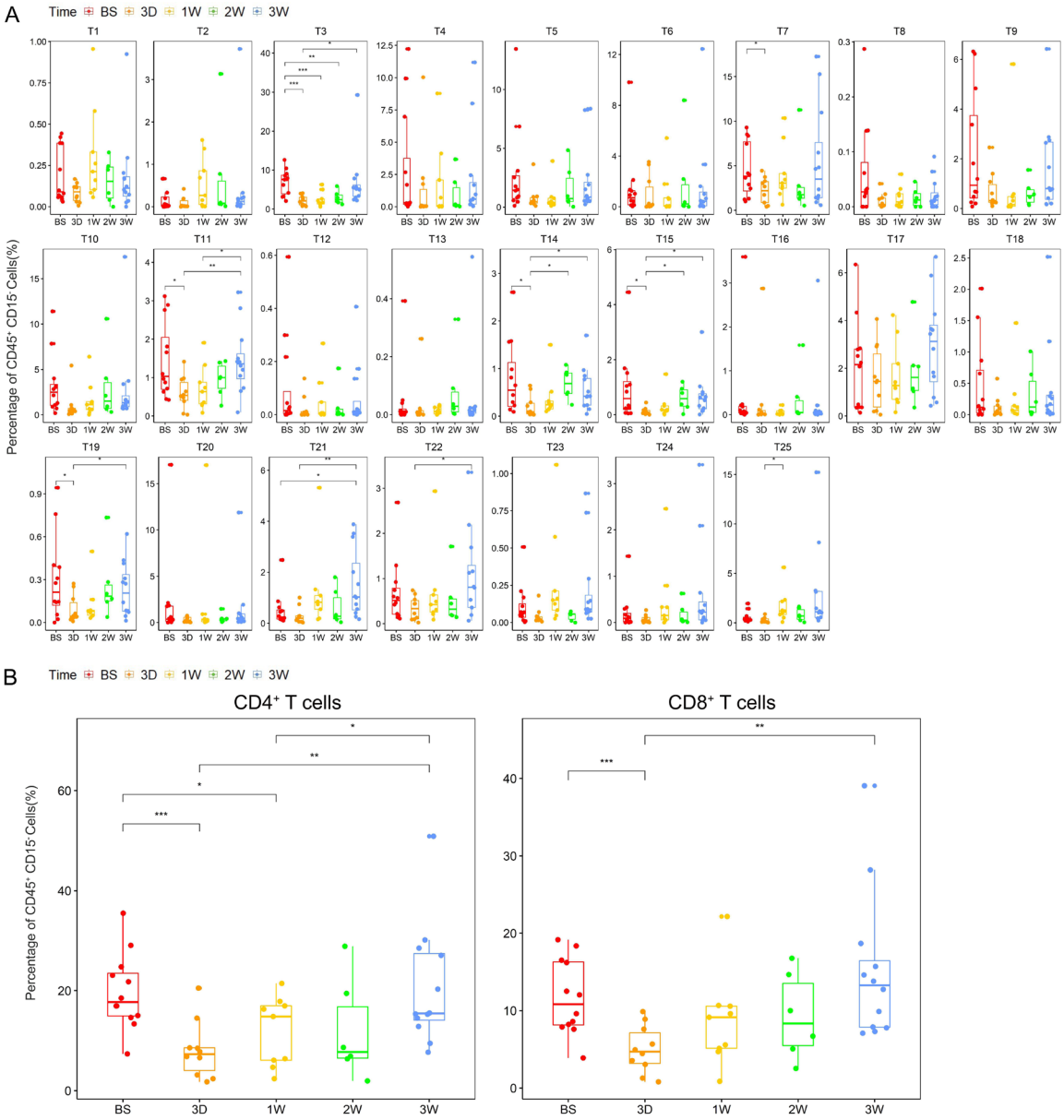

Figure S2. The peri-transplant frequency change of X-shift-defined T cell subsets. Box plots showing the percentage of indicated immune cell subsets at 5 peri-transplant time points (BS, 3D, 1W, 2W, and 3W), *P*-values were calculated by two-sided unpaired Student's T-test (*: P<0.05, **: P<0.01 and ***: P<0.001) The horizontal line of the box plot indicates the median, the boxes represent the interquartile range (IQR), and the whiskers reach to the farthest data within 1.5×IQR from the median. A: The frequency change of 25 T cell subsets. B: The frequency change of the total $CD4^+$ T cells (left), and $CD8^+$ T cells (right).

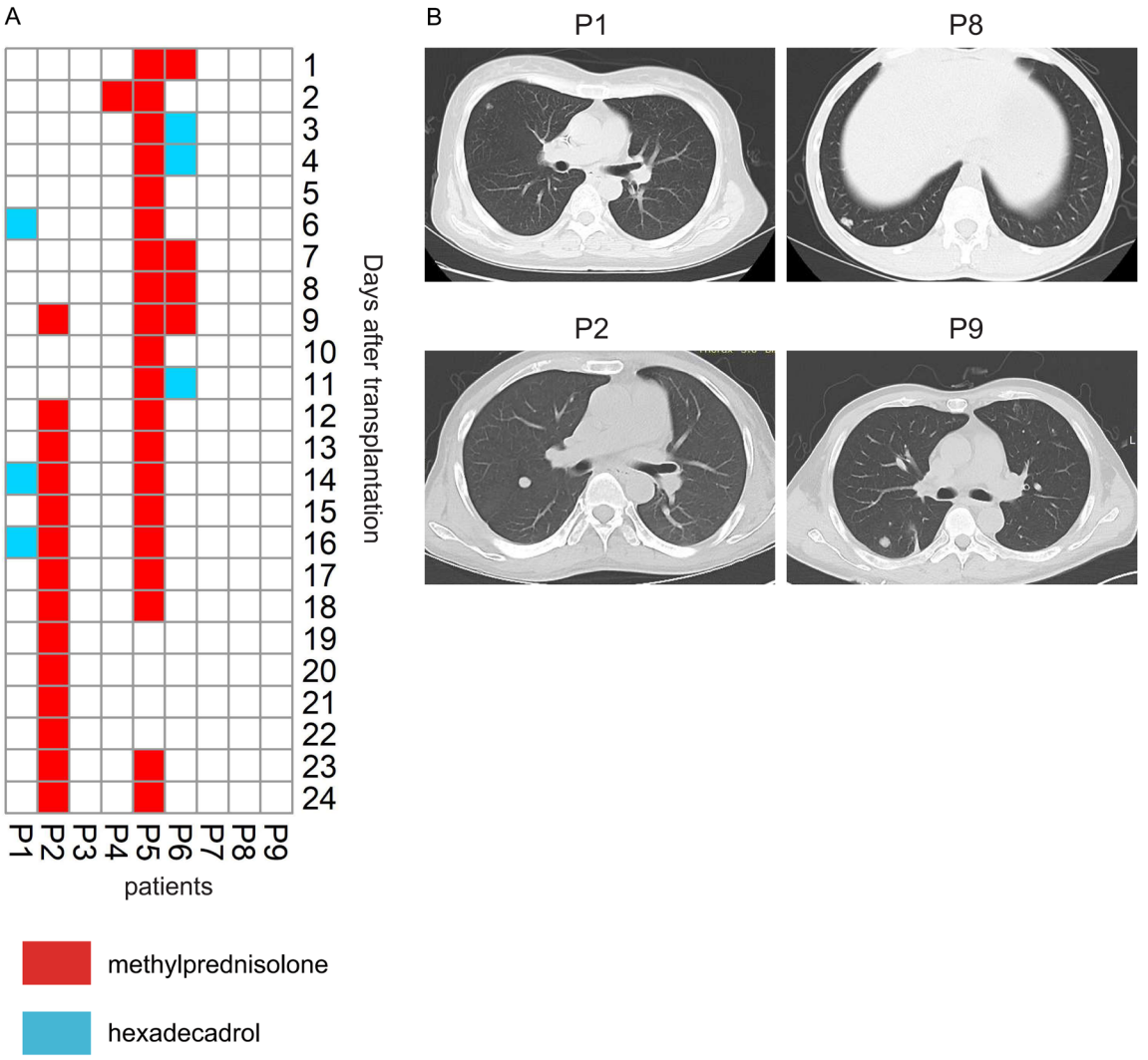

Figure S3. Relevant clinical information. A. Use of glucocorticoid for patients who received liver transplantation for hepatocellular carcinoma, cells are colored if the indicated glucocorticoid is applied. B. Computerized tomography (CT) Imaging verifying the tumor recurrence in four patients who received liver transplantation for hepatocellular carcinoma.

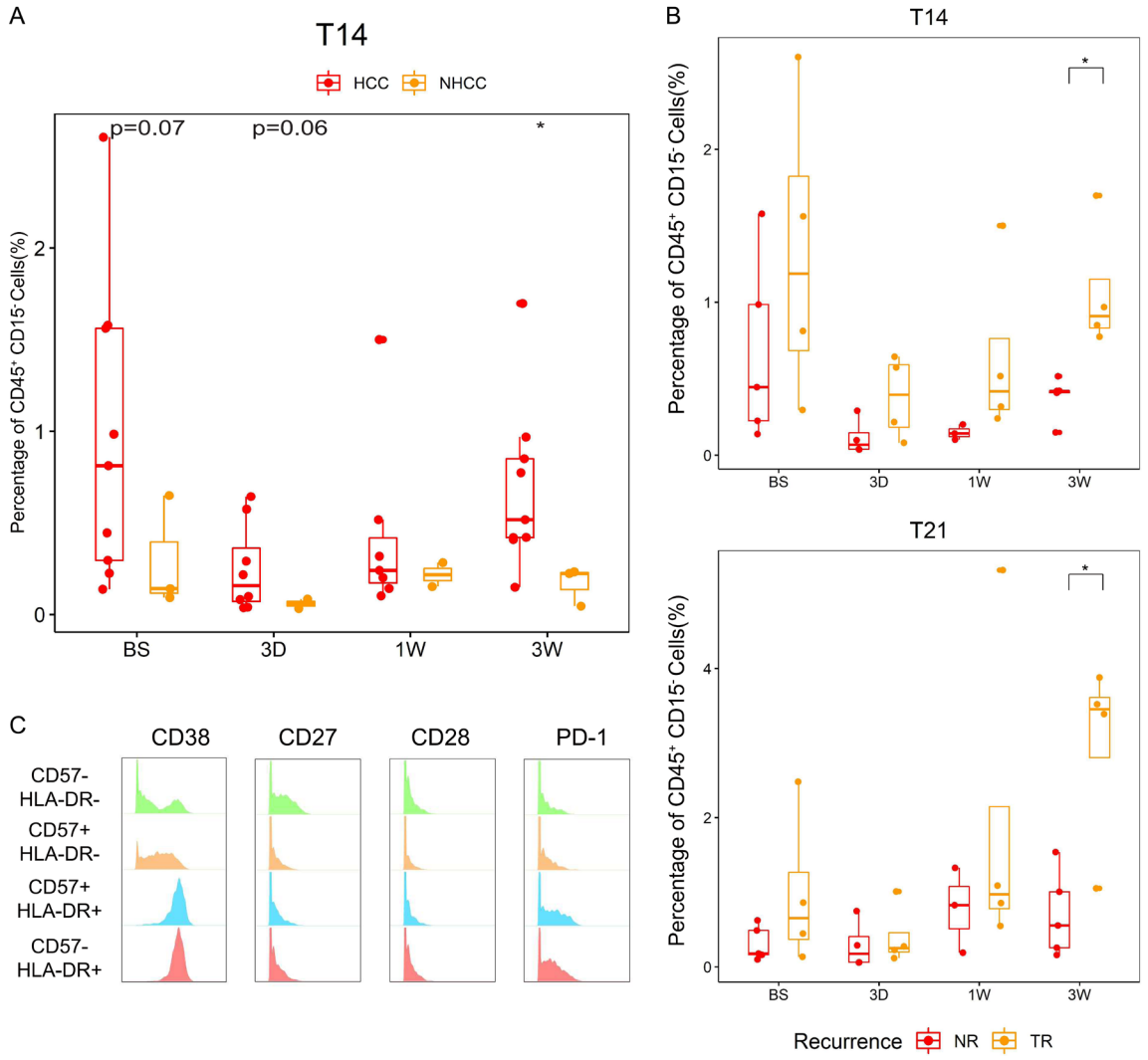

Figure S4. Frequency change and marker expression of X-shift-defined cluster T14 and T21 after liver transplantation (LT). A. Boxplots comparing the frequency of cluster T14 between patients receiving LT for hepatocellular carcinoma (HCC-LT) and patients receiving LT for other non-HCC reasons (NHCC-LT). B. Boxplots comparing the frequency of cluster T14 (up) and T21 (bottom) between HCC-LT recipients who developed tumor recurrence (TR) after transplantation and HCC-LT recipients with no tumor recurrence (NR). C. Histograms of cell distribution showing the expression level of indicated cytokines and functional biomarkers for $CD57^-$ $HLA\text{-}DR^-$ $CD8^+$ T cells, $CD57^-$ $HLA\text{-}DR^+$ $CD8^+$ T cells, $CD57^+$ $HLA\text{-}DR^-$ $CD8^+$ T cells, and $CD57^+$ $HLA\text{-}DR^+$ $CD8^+$ T cells. *P*-Values were calculated by two-sided unpaired Student's T-test (*: P<0.05, **: P<0.01 and ***: P<0.001) The horizontal line of the box plot indicates the median, the boxes represent the interquartile range (IQR), and the whiskers reach to the farthest data within 1.5×IQR from the median.

Table S7. Antibody information Mass-tag, clone, brands of antibodies used in the functional assessment panel

No.	mass-tag	antibody	Clone	Brand
1	89Y	CD45	HI30	BioLegend
2	115In	CD3	UCHT1	Bio X cell
3	139La	IFN-γ	B27	BioLegend
4	142Nd	gdTCR	5A6.E9	Home-made
5	145Nd	CD20	2H7	BioLegend
6	146Nd	CD123	6H6	BioLegend
7	148Nd	IL-2	MQ1-17H12	BioLegend
8	149Sm	IL-10	JES3-9D7	BioLegend
9	150Nd	IL-4	MP4-25D2	BioLegend
10	151Eu	IL-8	E8N1	BioLegend
11	152Sm	TNF-α	Mab11	BioLegend
12	153Eu	CD57	HCD57	BioLegend
13	156Gd	IL-13	JES10-5A2	BioLegend
14	159Tb	CD33	WM53	BioLegend
15	160Gd	CD28	CD28.2	BioLegend
16	161Dy	IL-17a	BL168	BioLegend
17	163Dy	CD68	Y1/82A	BioLegend
18	164Dy	CD38	HIT2	BioLegend
19	165Ho	IL-1b	8516	RD systems
20	166Er	Perforin	B-D48	Abcam
21	168Er	CD11c	BU15	BioLegend
22	169Tm	Ki-67	SolA15	eBioscience
23	171Yb	IL-9	MH9A4	BioLegend
24	172Yb	IL-21	3A3-N2	BioLegend
25	173Yb	Granzyme B	QA16A02	BioLegend
26	174Yb	PD-1	EH12.2H7	BioLegend
27	176Yb	HLA-DR	L243	BioLegend
28	197Au	CD4	RPA-T4	BioLegend
29	198Pt	CD8	RPA-T8	BioLegend
30	209Bi	CD11b	M1/70	Home-made

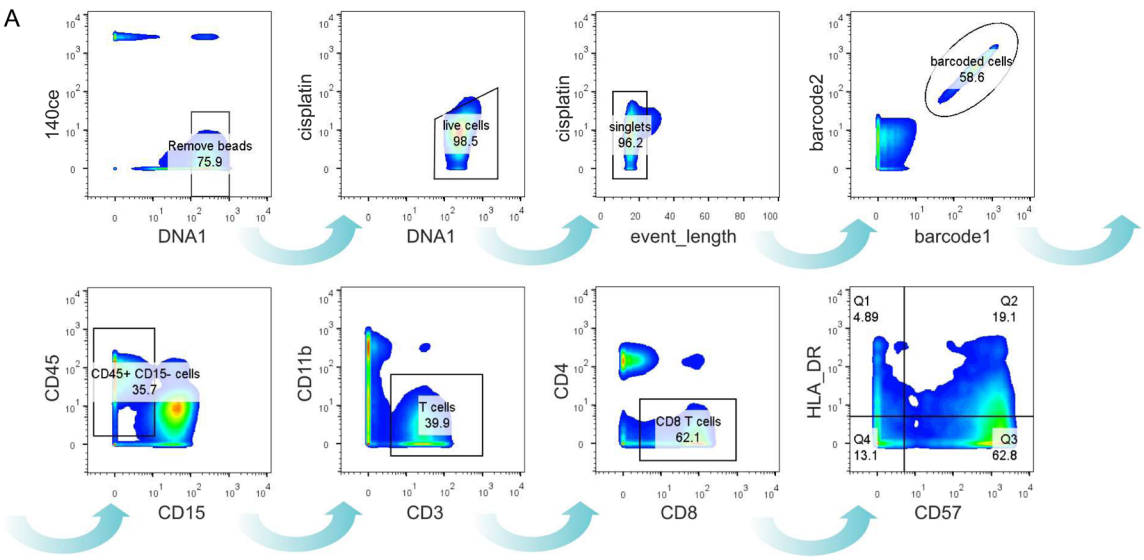
A
140ce
DNA1
Remove beads
75.9
cisplatin
DNA1
live cells
98.5
cisplatin
event_length
singlets
96.2
barcode2
barcode1
barcoded cells
58.6
CD45
CD15
CD45+ CD15- cells
35.7
CD11b
CD3
T cells
39.9
CD4
CD8
CD8 T cells
62.1
HLA_DR
CD57
Q1
4.89
Q2
19.1
Q4
13.1
Q3
62.8

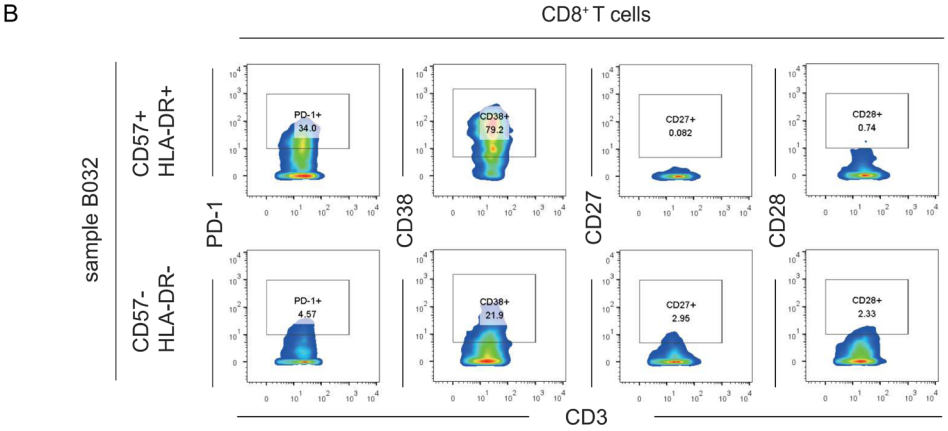
B
CD8⁺ T cells
sample B032
CD57+ HLA-DR+
CD57- HLA-DR-
PD-1
CD38
CD27
CD28
PD-1+ 34.0
CD38+ 79.2
CD27+ 0.082
CD28+ 0.74
PD-1+ 4.57
CD38+ 21.9
CD27+ 2.95
CD28+ 2.33
CD3

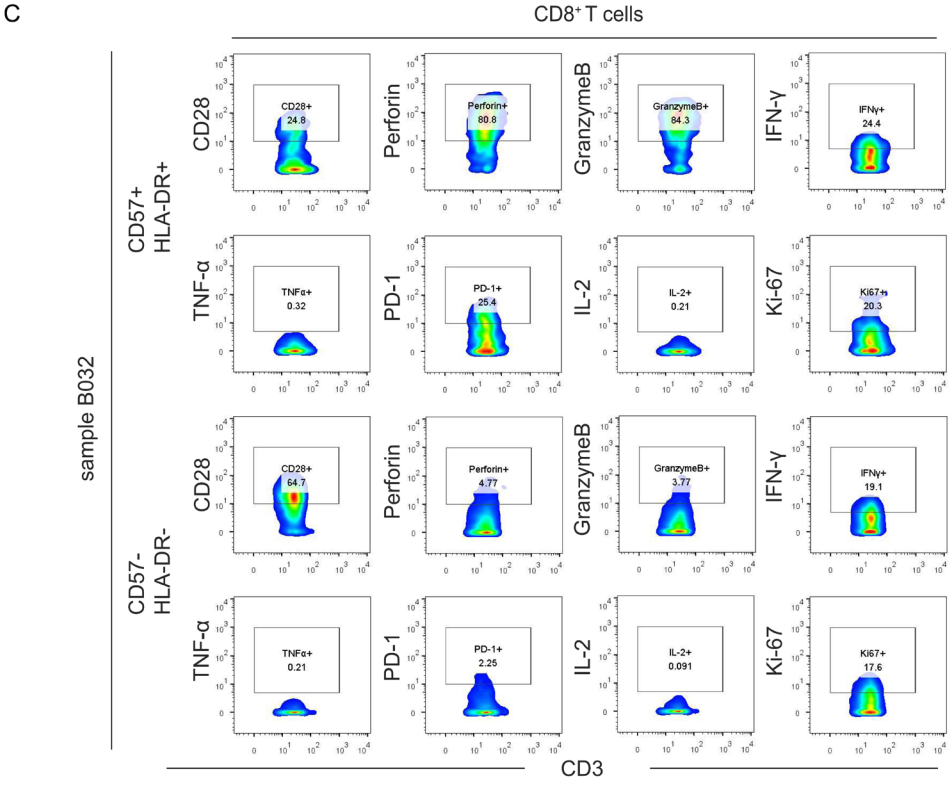
C
CD8⁺ T cells
sample B032
CD57+ HLA-DR+
CD57- HLA-DR-
CD28
Perforin
GranzymeB
IFN-γ
TNF-α
PD-1
IL-2
Ki-67
CD28+ 24.8
Perforin+ 80.8
GranzymeB+ 84.3
IFNγ+ 24.4
TNFα+ 0.32
PD-1+ 25.4
IL-2+ 0.21
Ki67+ 20.3
CD28+ 64.7
Perforin+ 4.77
GranzymeB+ 3.77
IFNγ+ 19.1
TNFα+ 0.21
PD-1+ 2.25
IL-2+ 0.091
Ki67+ 17.6
CD3

Figure S5. Gating strategy of CD57$^+$ HLA-DR$^+$ CD8$^+$ T cells (cluster T21). A. Pseudocolor contour plot depicting the gating strategy to obtain CD57$^+$ HLA-DR$^+$ CD8$^+$ T cells. B and C. Pseudocolor contour plot explaining how positive subsets of indicated biomarkers were defined.

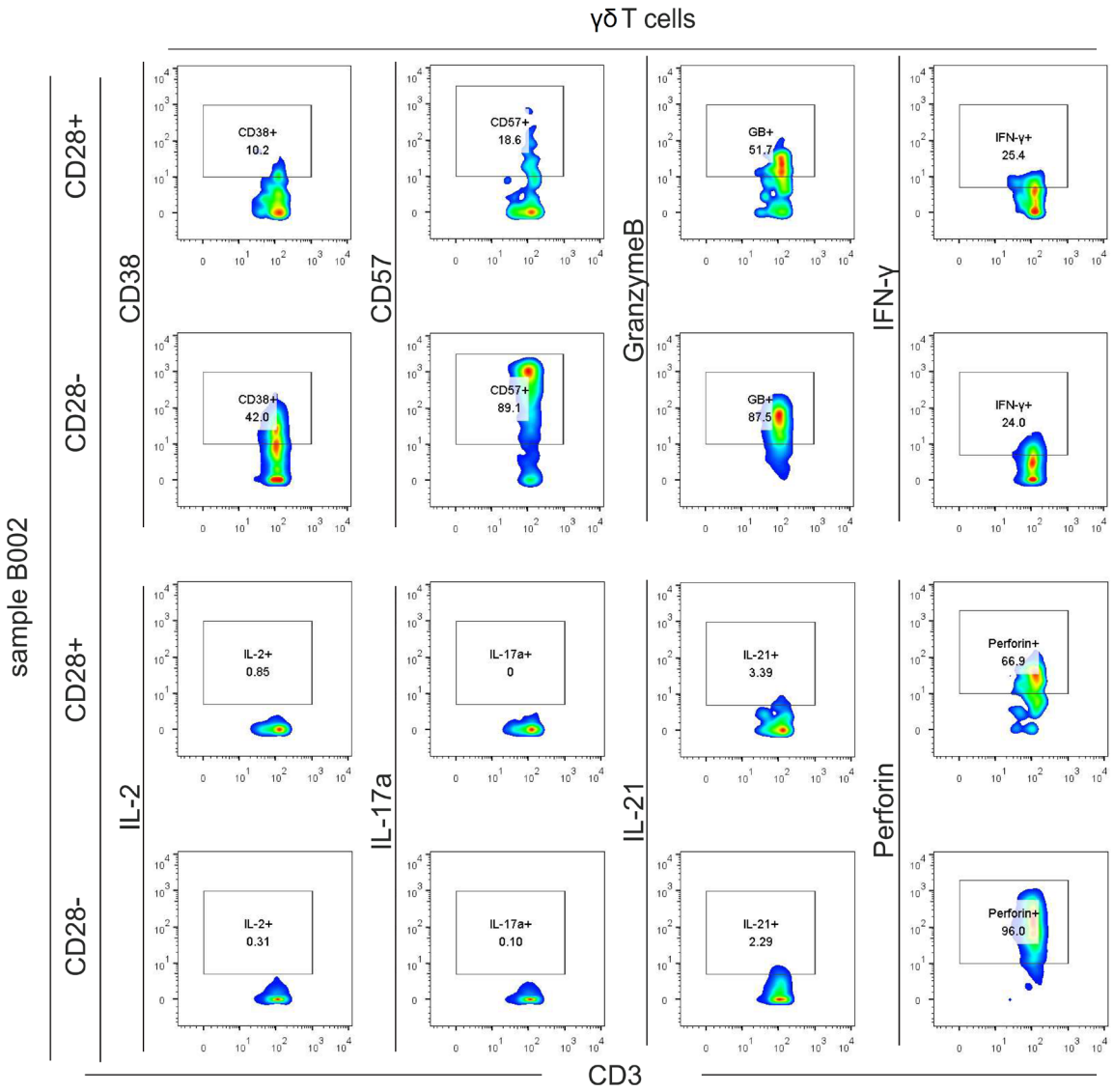

Figure S6. Gating strategy of CD28$^+$ γδ T cells (cluster T14). Pseudocolor contour plot explaining how positive subsets of indicated biomarkers were defined.